Identification of some novel pyrazolo[1,5-a]pyrimidine derivatives as InhA inhibitors through pharmacophore-based virtual screening and molecular docking.

Palmi Modi, Shivani Patel & Mahesh T Chhabria

Identification of some novel pyrazolo[1,5-*a*]pyrimidine derivatives as InhA inhibitors through pharmacophore-based virtual screening and molecular docking.

Palmi Modi[a,b], Shivani Patel[a,c], Mahesh T Chhabria[a]*

[a,]*Department of Pharmaceutical Chemistry, L. M. College of Pharmacy, Ahmedabad – 380009, Gujarat, India*
 [b]*Department of Pharmacy, Dharmsinh Desai University, Nadiad – 387001,Gujarat, India*
[c]*Division of biological and life sciences, Ahmedabad University, Ahmedabad – 380009, Gujarat, India*

*Corresponding author
Dr. Mahesh Chhabria
Principal,
L. M. College of Pharmacy, Ahmedabad
Gujarat, India
E-mail: mahesh.chhabria@rediffmail.com

Abstract:

The InhA inhibitors play key role in mycolic acid synthesis by preventing the fatty acid biosynthesis pathway. In this present article Pharmacophore modelling and molecular docking study followed by *in silico* virtual screening could be considered as effective strategy

to identify newer enoyl-ACP reductase inhibitors. Pyrrolidine carboxamide derivatives were opted to generate pharmacophore models using HypoGen algorithm in Discovery studio 2.1. Further it was employed to screen Zinc and Minimaybridge databases to identify and design newer potent hit molecules. The retrieved newer hits were further evaluated for their drug likeliness and docked against enoyl acyl carrier protein reductase. Here, novel pyrazolo[1,5-*a*]pyrimidine analogues were designed and synthesized with good yields. Structural elucidation of synthesized final molecules was perform through IR, MASS, ^{1}H-NMR, ^{13}C-NMR spectroscopy and further tested for its *in-vitro* anti-tubercular activity against H37Rv strain using Microplate Alamar blue assay (MABA) method. Most of the synthesized compounds displayed strong anti-tubercular activities. Further, these potent compounds were gauged for MDR-TB, XDR-TB and cytotoxic study.

Key words:

Enoyl acyl carrier protein reductase (InhA); pharmacophore modelling; virtual screening; molecular docking

Abbreviations:

TB; Tuberculosis; MDR-TB; Multi-Drug Resistant Tuberculosis; XDR-TB; Extensively Drug Resistant Tuberculosis; InhA; Enoyl acyl carrier protein reductase; PDB; Protein Data Bank; RMSD; Root Mean Square Deviation; RMSF; Root Mean Square Fluctuations; HBA; Hydrogen Bond Acceptor; RA; Ring Aromatic; HY; Hydrophibic; ADMET; Adsorption, Distribution, Metabolism, Disstribution, Toxicity.

Introduction

Tuberculosis (TB) is an airborne infectious disease caused by different species of *Mycobacterium tuberculosis*. It is one of the greatest health hitches with gradually increasing the mortality and morbidity (Tsukamura et al., 1978). Although effective chemotherapy has been placed over 50 years, world health organisation has declared tuberculosis "a global health emergency" which is the leading cause of death (Dye et al., 2009). Worldwide estimated 9.2 million people are infected with tuberculosis among them 4.9 million were men, 3.2 million women and 1.0 million children (Williams et al., 2005). Also 1.2 million new TB cases are living with HIV (Yang et al., 2006). There is one death from TB every 15 second (over two million per year). Now days, drug resistance strain of mycobacterium species has narrowed down the conventional anti-tuberculosis therapy. Development of resistance towards the first line drugs such as isoniazid (INH) and rifampicin is also significant concern (Banerjee et al., 1994). Thus, there is an urgent need to develop newer therapeutic entities with different mechanism of action as an anti-tubercular agent. Pathogenicity of *Mycobacterium tuberculosis* is linked with its peculiar nature of cell envelope which possesses two fatty acid synthase (FAS) pathways FAS-I and FAS-II. These pathways are involved for synthesis of mycolic acids. Mycolic acids, the key constituent for cell wall biosynthesis with 60-90 carbons of α-alkyl β-hydroxyl fatty acids (Takayama et al., 2005). Enoyl-ACP reductase (InhA) of *Mycobacterium tuberculosis* participates by blocking the fatty acid biosynthesis pathway (FAS II) (Asselineau et al., 1950). For the synthesis of mycolic acid it utilises the NADH cofactor as a hydrogen bond donor to reduce the trans double bond conjugated to the carbonyl group of long chain fatty acid (Zhang et al., 1993 and Quemard et al., 1995). Substantial number of strains are unaffected to INH develop mutation in KatG, a catalase-peroxidase enzyme with twofold activities peroxidase oxidizing to form INH-NAD adduct at the 4th position and catalase (Zhang et al., 1992 and Zhao et al., 2006). As there are limited numbers of drugs available to treat tuberculosis, there is a crucial requirement to develop medicinally useful enoyl acyl carrier protein reductase (InhA) inhibitors as newer anti-tubercular drug. So, it is a target of choice for the expansion of newer anti-tubercular agents.

Recently in the past, several efforts have been made to discover novel InhA inhibitors combined with *in-silico* virtual screening, molecular dynamics simulations and quantum chemical (Mohsin et al., 2017) as well *in-vitro* analysis against *Mycobacterium tuberculosis* H37Rv strain (Mohsin et al., 2017). But, only a few of them have shown the prominent response to *in-vitro* anti-tubercular study. Based on the requirement for the potent anti-

tubercular agents, we have applied combination of ligand based pharmacophore modelling and structure based molecular docking study to identify newer InhA inhibitors. Ligand based pharmacophore strategy was applied with novel class of pyrolidine carboxamides as InhA inhibitors (He et al., 2007). The best generated pharmacophore model was used to screen database which retrieved structurally companionable potential hits. On the basis of virtual screening we have designed newer class of pyrazolo[1,5-*a*]pyrimidine analogues. This newer analogues were further evaluated for their drug likeness properties using QikProp (Schrodinger Inc., USA). Molecular docking study was carried out using co-crystal structure of enoyl-ACP reductase (PDB Code: 2H7M) to identify the essential binding modes. Anti-tubercular activity of these synthesized compounds was performed through Microplate Alamar Blue Assay (MABA) Method. Potent hit molecules from preliminary screening were further opted for MDR-TB, XDR-TB and cytotoxicity study.

Materials and methods

Pharmacophore modelling

Dataset

Series of Pyrrolidine carboxamide derivatives with known biological activity were used as a dataset to generate the pharmacophore model (He et al., 2006). One of the important criteria for generation of pharmacophore model is that the activity data must be derived from the same bioassay method, represented in same term and have wide range in biological activity. Selected pyrrolidine carboxamide series has all these characteristics and thus selected for this study. Structural diversity and biological activity with the 5-6 orders of magnitude were also important criteria for the selection of the training set and test set **(Table S1, Supplementary information)**. Compounds which do not have activity in real number were omitted (Shalini et al., 2017).

Generation of the pharmacophore model

This approach signifies the 3D pharmacophore design including chemical features derived from the datasets of molecules which were previously reported as InhA inhibitors. In present study, discovery studio 2.1 was used to construct and visualise the pharmacophore models (He et al., 2006). All the Structures were optimised using CHARMm force field. Pooling algorithm was employed to find out the best conformations. The "Best conformer generation" method was carried with energy cut off 29kcal/mole and maximum 255 conformers were generated.

Generation of 3D pharmacophore model was carried out in following three steps:

a) Selection of training set molecules with the activity span of 5-6 orders of magnitude to generate 3D structures; b) Generation of the pharmacophore by selecting appropriate pharmacophoric features. The pharmacophore was generated using HypoGen module by considering the important features of enoyl-ACP reductase inhibitors. Hydrogen bond acceptor (HBA), ring aromatic (RA) and hydrophobic (HY) were the well-defined features for the generation of the pharmacophore model. The minimum numbers of features were varied from 0 to 5 to achieve a statistically significant model; and c) Conformation search was carried out to find novel entities form the databases (Rao et al., 2008). Further to achieve final pharmacophore model selected features were refined and trimmed manually accompanying the important residues with "Edit and cluster pharmacophore features" protocol in the tool panel.

Pharmacophore validation

Pharmacophore validation was performed to check whether generated models are adequate to predict the active compounds or not. It was collectively performed by evaluating the cost analysis: fixed cost, total cost, null cost, configuration cost, Fischer randomization (known as Y-scrambling) and external predictability of the model (ability to predict biological activity of the test set compounds). In the cost analysis, fixed cost is the cost of theoretically ideal pharmacophore model with representation of the simplest model to fit all the data perfectly. Null cost presumes no statistically significant structure in the data and the experimental activities are normally distributed around their mean (Mason et al., 2001). The weight cost, error cost and configuration cost is sum of the total cost. The weight cost (sum of feature weight) increases in a Gaussian form which should be deviated from its ideal value 2.0 (Mason et al., 2001). The error cost value increases with the increase in root mean square difference between estimated and measured activity. The configuration cost is a fixed cost signifies the complexity and entropy of the total assumed pharmacophoric space which should always be less than 17 (Santo et al., 2005). For the statistical relevance of the model Fischer's randomization test was employed to revalidate the model. Activities of the training set molecules were reassigned using Fischer's randomization at statistical significance levels of 95% to generate 19 random spread sheets. Further, the predictability of the model was checked by 17 test set molecules and minimized using CHARMm forcefield in the Discovery Studio. Mapping of the test set molecules was performed with "Ligand pharmacophore Mapping" protocol using "Best Mapping only" and rigid "Fitting Method". Rigid "Fitting Method was applied for the test set molecules to achieve defined estimated biological activity (IC$_{50}$ in μM) by Hypo 1.

Virtual screening

Virtual screening is an efficient tool used to find chemically diverse and potential leads. Two databases: MiniMaybridge and ZINC database were screened by employing validated pharmacophore model as 3D query (Funk et al., 2004). The pharmacophore search results were sorted according to fit value. The "Maximum omitted features" was set to 1. Hit compounds with higher fit values and better estimated biological activity IC_{50} in μM predicted using Hypo 1 model were subjected for their drug likeness properties using QikProp module.

Identification of the best protein for docking

Six co-crystallised enoyl-ACP reductase proteins (PDB IDs: 2H7I, 2NSD, 2H7M, 2B36, 3FNG, 2H7L) are available with different resolutions and co-crystal structure in the protein data bank. All 3D protein structure has 100% sequence similarity. So, before carrying out the molecular docking protocol it is necessary to identify the best protein for further study based on RMSD value between docked confirmation of ligand and co-crystal ligand also having lower binding energies. The crystal ligands were grouped and redocked to verify essential hydrogen bonding interactions with Tyr158 and NAD^+. These ligands were Cross dock against the listed protein to identify variable binding poses with significantly differing binding energies using Glide. The average RMSD was calculated with respect to each protein ligand pose. Structural alignment was also performed with co-crystalline structures. Here alignment of all the PDBs have been performed to identify the exact binding mode of the co-crystal structure to PDB. The X-ray structure with their exact binding modes and reasonable low binding energies compared to other structures is further selected for the molecular docking study. Structural alignment of 2H7I and 2H7M proteins **Figure 1** and their alignment score was also calculated **Table 1**. On the basis of lower RMSD and good alignment score 2H7M protein was further employed for molecular docking study.
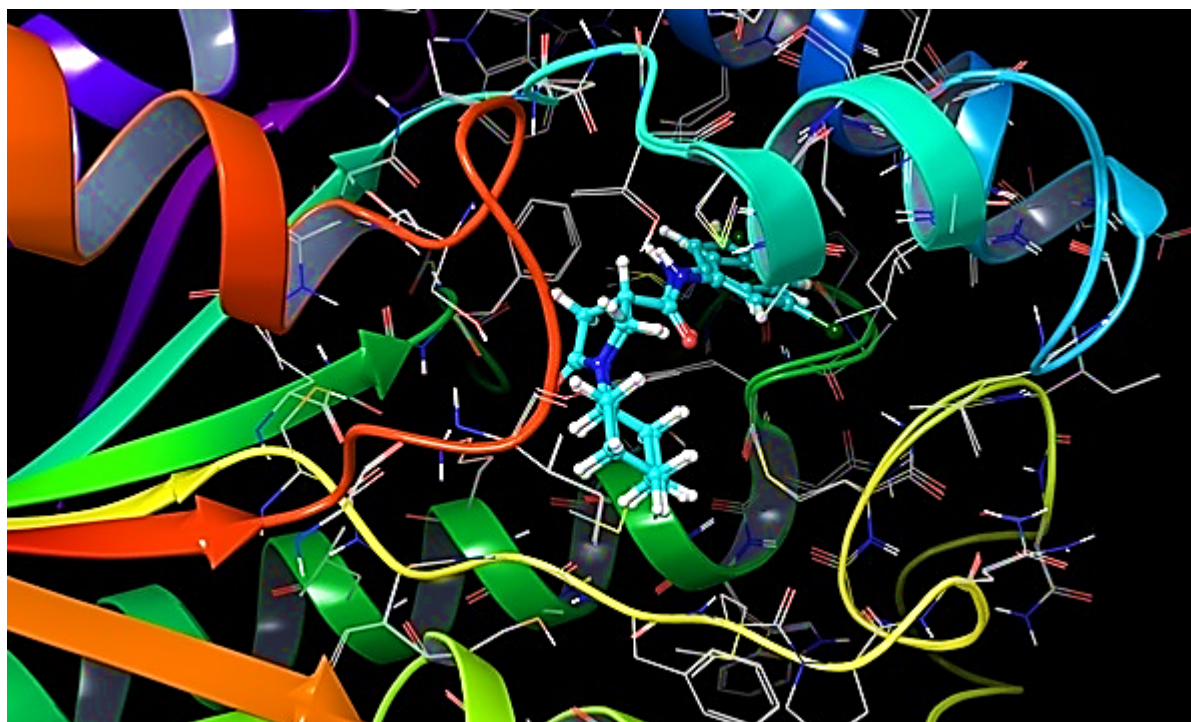
Figure 1 Crystal structures of 2H7M and 2H7I overlaid on each other. Conformational changes of aliphatic side chains on binding of different ligands are evident. Protein residues in lines, ligands in ball and sticks.

Table 1 Alignment score and RMSDs of different X-ray crystal structures of InhA protein

Sr. No.	PDB Codes	Alignment Score	RMSD
1	3FNG-2B36	0.036	0.943
2	2B36-2H7L	0.020	0.715
3	2H7L-2H7I	0.01	0.136
4	2H7I-2H7M	0.01	0.118
5	2H7M-2NSD	0.020	0.682

Protein preparation and grid generation

Protein structure was prepared using the Protein Preparation Wizard in Maestro (Maestro v.10.1). Default settings were used, except that missing side chains were added, water molecules were removed from the crystal structure beyond 5 Ǻ. Exhaustive sampling was done to refine the protein structure in order to obtain better H-bond assignment. Receptor grid

was generated using "Glide's Receptor Grid Generation" module with the default parameter of van der Waals scaling factor and charge cut off. A centred dimension cubic box of 10 Å × 10 Å × 10 Å was generated with the help of OPLS 2005 force field at the active site of the co-crystalline ligand.

Molecular Docking

Extra precision (XP) docking was carried out with flexible ligands to identify the essential amino acid residual interaction (Irwin et al., 2012). Van der Waals scaling factor and partial charge cut off was selected for ligand atoms (Maestro v10.1 Glide, 2009). Energy-minimized poses of the virtual hit ranked by Glide score. Minimum 10 poses were generated for each ligand (Podlogar et al., 2000). Molecular docking via computer aided-drug design approach plays a vital role in the designing of potential ligands with compatible binding site of desired targeted molecules. Co-crystallised enoyl-ACP reducates proteins (PDB IDs: 2H7M) were selected and extracted from protein data bank (PDB http://www.rcsb.org/pdb) (Sivakumar et al., 2007). To refine the protein default settings were applied structural hydrogen atoms were added and water molecules were removed beyond 5Å followed by minimization with OPLS 2005 force field. Further the crystal ligand was extracted and "Glide's Receptor Grid Generation" protocol was applied to generate the receptor grid with cubic box of 10 Å × 10 Å × 10 Å dimensions at the active site of the co-crystalline ligand (Halgren et al., 2004). Predicted designed NCE's (6a-6i) surviving to the Lipinski's rule of five were docked using Glide Standard precision (SP) protocol to study the predicted essential amino acid residual interaction (Maestro v10.1, Schrodinger, LLC, NEW YORK, NY).

Chemistry

All Laboratory grade solvents and chemicals were purchased from commercial suppliers, Spectrochem Pvt. Ltd., Rankem India Ltd. and Sigma Aldrich. Thin layer chromatography was performed for monitoring the completion of the reaction. Melting points were obtained by open capillary method on VEEGO VMP-D model and are uncorrected. Infrared (IR) spectra were recorded in KBr using FT-IR 8400S Shimadzu Fourier Transform spectrophotometer. Mass spectra were recorded on Perkin-Elmer LC-MS PE Sciex API/65. ^{1}H NMR spectra and ^{13}C NMR were taken on Bruker Advance 400 spectrophotometer and the chemical shifts are given as parts per million (ppm) downfield from tetramethylsilane (TMS) as internal standard.

Synthesis

General procedure for the synthesis of 2-cyano-N-(substituted phenyl)acetamide (2)

Different substituted amines (0.0468 mol) was added to ethyl cyanoacetate (0.0468 mol) in a round bottom flask and refluxed for 8 hours using DMF as a solvent. Completion of the reaction was monitored by TLC. After the completion of the reaction, mixture was poured into ice-cold water. The solid obtained was filtered and dried. The crude product was recrystallized from ethanol to yield pure crystalline solid.

General procedure for the synthesis of 2-cyano-N-(substituted phenyl)-3,3bis(methylthio)acrylamide (3)

To the solution of potassium hydroxide (0.01046mol, 0.59 g) in 5 ml water, 2-cyano-*N*-(substituted phenyl)acetamide (0.00523 mol, 1 g) was added with continuous stirring and cooled at 0-5°C. To this solution 15 ml of DMF was added, and carbon disulphide (0.00523mol, 0.397 g) was added drop wise. Reaction mixture was allowed to stirr for 30 minutes and dimethylsulphate (0.01046mol, 1.34 g) was added drop wise. The reaction mixture was stirred for 2 hours and further poured into ice-water mixture. The solid obtained was filtered, washed with water and dried. Recrystallized from methanol yielded colorless crystalline product.

General procedure for the synthesis of 2-cyano-3-(methylthio)-N-substituted phenyl-3-(substituted phenylamino)acrylamide (4)

2-cyano-*N*-(substituted phenyl)-3,3bis(methylthio)acrylamide (1.0 g, 0.003 mol) was dissolved in 10 ml IPA. Different substituted aniline (0.67 g, 0.003 mol) was added to the reaction mixture and the mixture was refluxed for 14-15 hours. The reaction was monitored by TLC. After completion of the reaction, mixture was poured into ice cold water. Solid obtained was filtered and dried. Recrystallized it from IPA yielded crystalline product.

General procedure for the synthesis of 5-amino-N-substituted phenyl-3-(substituted phenylamino)-1H-pyrazole-4-carboxamide (5)

To the solution of 2-cyano-3-(methylthio)-N-substituted phenyl-3-(substituted phenylamino)acrylamide (1g, 0.0104 mol) in 20 ml ethanol hydrazine hydrate (0.62 ml, 0.0104 mol) was added. The reaction mixture was refluxed for 3-4 hours and completion of the reaction was monitored by TLC. After completion of the reaction, ethanol was distilled off until the solid was obtained. Solid was filtered and dried. Recrystallized it from ethanol to yield pure crystalline product.

General procedure for the synthesis of 7-hydroxy-5-methyl-N- substituted phenyl-2-(substituted phenylamino)pyrazolo[1,5-a]pyrimidine-3-carboxamide (6)

To the crystalline solid product of 5-amino-N-substituted phenyl-3-(substituted phenylamino)-1H-pyrazole-4-carboxamide (1g, 0.001029 mol) ethyl aceto acetate (0.7 ml,

0.01029 mol) was added and refluxed in oil bath for 1 hours. Completion of the reaction was monitored by TLC. Solid separated out from the reaction mixture was filtered. Recrystallized from chloroform to yielded pure crystalline product.

Spectral Characteristics

N-(3-chlorophenyl)-7-hydroxy-2-((4-methoxyphenyl)amino)-5-methylpyrazolo[1,5-a]pyrimidine-3-carboxamide (6a)

M.P. 262-264°C; Yield, 82%; IR spectra (KBr, cm^{-1}) 3353 (-NH str.), 1660 (-CO-NH str.), 1245 (-C-N str.), 813 (P-substituted), 775 (-C-Cl str.); Calculated (M/Z): 407.1; Obtained MS: 407.1 (M), 409. 4 (M+2); ^{1}H NMR (400 MHz, DMSO-d$_6$, δ, ppm): δ 12(s, 1H, OH-Ar., D$_2$O exchangeable), δ 9.8(s, 1H, C-O-NH-Ar., D$_2$O exchangeable), δ 8.8 (s, 1H, NH-Ar., D$_2$O exchangeable), δ 5.5-8.1(m, 7H,-CH-Ar.), δ 5.7(s, 1H,-CH-Ar.), δ 2.3(s, 3H, -CH$_3$-Ar), δ 2.2(s, 3H, -CH$_3$-Ar); ^{13}C NMR (400 MHz, DMSO-d$_6$, δ, ppm): 162.20, 154.96, 153.71, 140.18, 138.86, 136.17, 132.80, 130.22, 125.61, 123.06, 122.91, 122.70, 120.08, 119.05, 115.47, 98.33, 87.14, 20.45, 12.92

2-((3-chloro-4-fluorophenyl)amino)-7-hydroxy-N-(4-methoxyphenyl)-5 methylpyrazolo[1,5-a]pyrimidine-3-carboxamide (6b)

M.P. 268-271°C; Yield, 67%; IR spectra (KBr, cm^{-1}) 3390 (-NH str.), 1616 (-CO-NH str.), 1215 (-C-N str.), 1163 (-C-F str.), 1037 (-C-O-C), 867 (D-substituted), 833 (P-substituted), 773 (-C-Cl str.);Calculated (M/Z): 441.1; Obtained MS: 442.9 (M+1); ^{1}H NMR (400 MHz, DMSO-d$_6$, δ, ppm): δ 12(s, 1H, OH-Ar., D$_2$O exchangeable), δ 9.8(s, 1H, C-O-NH-Ar., D$_2$O exchangeable), δ 8.8 (s, 1H, NH-Ar., D$_2$O exchangeable), δ 5.5-8.1(m, 8H,-CH-Ar.), δ 5.7(s, 1H,-CH-Ar.), δ 2.3(s, 3H, -CH$_3$-Ar); ^{13}C NMR (400 MHz, DMSO-d$_6$, δ, ppm):161.22, 155.57, 154.82, 153.49, 153.21, 147.20, 140.30, 134.42, 131.59, 122.56, 118.60, 114.04, 113.61, 98.14, 87.33, 55.15, 18.79

2-((4-fluorophenyl)amino)-7-hydroxy-N-(4-methoxyphenyl)-5-methylpyrazolo[1,5-a]pyrimidine-3-carboxamide (6c)

M.P. 276-278°C; Yield, 56%; IR spectra(KBr, cm^{-1}) 3402 (-NH str.), 1616 (-CO-NH str.), 1218 (-C-N str.), 1081 (-C-F str.), 1041 (-C-O-C), 829 (P-substituted); Calculated (M/Z): 407.1; Obtained MS: 408.5 (M+1); ^{1}H NMR (400 MHz, DMSO-d$_6$, δ, ppm): δ 11.9(s, 1H, OH-Ar., D$_2$O exchangeable), δ 9.9(s, 1H, C-O-NH-Ar., D$_2$O exchangeable), δ 8.8 (s, 1H, NH-Ar., D$_2$O exchangeable), δ 6.9-7.7(m, 8H,-CH-Ar.), δ 5.7(s, 1H,-CH-Ar.), δ 3.7(s, 3H, -CH$_3$-Ar), δ 2.5(s, 3H, -CH$_3$-Ar); ^{13}C NMR (400 MHz, DMSO-d$_6$, δ, ppm): 161.22, 155.57, 154.82, 153.49, 153.21, 147.20, 140.30, 134.42, 131.59, 122.56, 118.60, 114.04, 113.61, 98.14, 87.33, 55.15, 18.79

2-((3-chlorophenyl)amino)-7-hydroxy-N-(4-methoxyphenyl)-5-methylpyrazolo[1,5-a]pyrimidine-3-carboxamide (6d)

M.P. 210-213°C; Yield, 72%; IR spectra (KBr, cm^{-1}) 3305 (-NH str.), 1658 (-CO-NH str.), 1253 (-C-N str.), 1041 (-C-O-C), 819 (*P*-substituted), 773 (-C-Cl str.); Calculated (M/Z): 423.1; Obtained MS: 424.2 (M+1), 426. 4(M+2); ^{1}H NMR (400 MHz, DMSO-d$_6$, δ, ppm): δ 12(s, 1H, OH-Ar., D$_2$O exchangeable), δ 9.5(s, 1H, C-O-NH-Ar., D$_2$O exchangeable), δ 8.7 (s, 1H, NH-Ar., D$_2$O exchangeable), δ 6.9-7.6(m, 8H,-CH-Ar.), δ 5.7(s, 1H,-CH-Ar.), δ 2.5(s, 3H, -CH$_3$-Ar), δ 2.3(s, 3H, -CH$_3$-Ar); ^{13}C NMR (400 MHz, DMSO-d$_6$, δ, ppm): 162.20, 155.57, 154.82, 153.49, 153.21, 147.20, 140.30, 134.42, 131.59, 122.56, 118.60, 114.04, 113.61, 98.14, 87.33, 55.15, 18.79

2-((3-chloro-4-fluorophenyl)amino)-7-hydroxy-5-methyl-N-phenylpyrazolo[1,5-a]pyrimidine-3-carboxamide (6e)

M.P. 281-282°C; Yield, 48%; IR spectra (KBr, cm^{-1}) 3375 (-NH str.), 1628 (-CO-NH str.), 1232 (-C-N str.), 1049 (-C-F str.), 900 (D-substituted), 819 (*P*-substituted), 765 (-C-Cl str.); Calculated (M/Z): 411.09; Obtained MS: 411.1 (M+1); δ 11.9(s, 1H, OH-Ar., D$_2$O exchangeable), δ 9.7(s, 1H, C-O-NH-Ar., D$_2$O exchangeable), δ 8.8(s, 1H, NH-Ar., D$_2$O exchangeable), δ 6.9-7.6(m, 8H,-CH-Ar.), δ 5.7(s, 1H,-CH-Ar.), δ 2.3(s, 3H, -CH$_3$-Ar); ^{13}C NMR (400 MHz, DMSO-d$_6$, δ, ppm): 161.22, 154.81, 152.42, 150.09, 140.48, 139.94, 138.71, 128.90, 128.72, 128.51, 128.47, 123.81, 123.54, 120.75, 118.97, 118.66, 98.16, 88.05, 18.85, 16.71

7-Hydroxy-N-(4-methoxyphenyl)-2-((4-methoxyphenyl)amino)-5-methylpyrazolo[1,5-a]pyrimidine-3-carboxamide (6f)

M.P. 280-282°C; Yield, 83%; IR spectra (KBr, cm^{-1}) 3363 (-NH str.), 1662 (-CO-NH str.), 1244 (-C-N str.), 1037 (-C-O-C), 825 (*P*-substituted); Calculated (M/Z): 389.1; Obtained MS: 390.5 (M+1), 391.5 (M+2); ^{1}H NMR (400 MHz, DMSO-d$_6$, δ, ppm): δ 11.9(s, 1H, OH-Ar., D$_2$O exchangeable), δ 9.7(s, 1H, C-O-NH-Ar., D$_2$O exchangeable), δ 8.5(s, 1H, NH-Ar., D$_2$O exchangeable), δ 6.8-7.6(m, 9H,-CH-Ar.), δ 5.7(s, 1H,-CH-Ar.), δ 3.7(s, 3H, -CH$_3$-Ar), δ 2.3(s, 3H, -CH$_3$-Ar); ^{13}C NMR (400 MHz, DMSO-d$_6$, δ, ppm): 161.22, 154.81, 152.42, 150.09, 140.48, 139.94, 138.71, 128.90, 128.72, 128.51, 128.47, 123.81, 123.54, 120.75, 118.97, 118.66, 98.16, 88.05, 55.15, 18.85

7-hydroxy-2-((4-methoxyphenyl)amino)-5-methyl-N-phenylpyrazolo[1,5-a]pyrimidine-3-carboxamide (6g)

M.P. 284-283°C; Yield, 78%; IR spectra(KBr, cm^{-1}) 3371 (-NH str.), 1635 (-CO-NH str.), 1211 (-C-N str.), 1059 (-C-F str.), 829 (*P*-substituted); Calculated (M/Z): 395.1; Obtained

MS: 396.2 (M+1); ^{1}H NMR (400 MHz, DMSO-d_6, δ, ppm): δ 11.9(s, 1H, OH-Ar., D_2O exchangeable), δ 9.9(s, 1H, C-O-NH-Ar., D_2O exchangeable), δ 9.7(s, 1H, NH-Ar., D_2O exchangeable), δ 6.4-9.2(m, 8H,-CH-Ar.), δ 5.8(s, 1H,-CH-Ar.), δ 2.5(s, 3H, -CH$_3$-Ar); ^{13}C NMR (400 MHz, DMSO-d_6, δ, ppm): 161.38, 157.71, 155.36, 154.74, 152.61, 150.01, 140.67, 140.37, 137.43, 132.76, 130.15, 123.02, 119.93, 118.86, 118.75, 118.68, 115.27, 115.05, 98.27, 87.73, 18.85

5-amino-N-(4-fluorophenyl)-3-((4-fluorophenyl)amino)-1H-pyrazole-4-carboxamide (6h)

M.P. 297-300°C; Yield, 63%; IR spectra (KBr, cm^{-1}) 3365 (-NH str.), 1662 (-CO-NH str.), 1222 (-C-N str.), 1026 (-C-O-C), 867 (D-substituted), 813 (*P*-substituted); Calculated (M/Z): 417.1; Obtained MS: 418.2 (M+1); ^{1}H NMR (400 MHz, DMSO-d_6, δ, ppm): δ 11.7(s, 1H, OH-Ar., D_2O exchangeable), δ 9.0(s, 1H, C-O-NH-Ar., D_2O exchangeable), δ 8.9(s, 1H, NH-Ar., D_2O exchangeable), δ 6.8-7.5(m, 7H,-CH-Ar.), δ 5.8(s, 1H,-CH-Ar.), δ 3.7(s, 3H, -OCH$_3$-Ar), δ 2.4(s, 3H, -CH$_3$-Ar.), δ 2.3(s, 6H, -CH$_3$-Ar.); ^{13}C NMR (400 MHz, DMSO-d_6, δ, ppm): 161.79, 155.70, 153.71, 138.99, 136.17, 131.38, 125.68, 122.86, 122.67, 122.56, 115.24, 113.72, 55.20, 20.47, 18.81, 12.91

5-amino-N-(2,4-dimethylphenyl)-3-((2-methoxyphenyl)amino)-1H-pyrazole-4-carboxamide (6i)

M.P. 199-203°C; Yield, 67%; IR spectra (KBr, cm^{-1}) 3305 (-NH str.), 1660 (-CO-NH str.), 1255 (-C-N str.), 1099 (-C-F str.), 871 (D-substituted), 813 (*P*-substituted), 775 (-C-Cl str.); Calculated (M/Z): 445.02; Obtained MS: 445.2 (M), 447.3 (M+2), 449.3 (M+4); ^{1}H NMR (400 MHz, DMSO-d_6, δ, ppm): δ 11.9(s, 1H, OH-Ar., D_2O exchangeable), δ 9.9(s, 1H, C-O-NH-Ar., D_2O exchangeable), δ 8.5(s, 1H, NH-Ar., D_2O exchangeable), δ 6.8-7.9(m, 7H,-CH-Ar.), δ 5.7(s, 1H,-CH-Ar.), δ 3.5(s, 3H, -CH$_3$-Ar), δ 2.3(s, 6H, -CH$_3$-Ar.); ^{13}C NMR (400 MHz, DMSO-d_6, δ, ppm): 161.50, 154.89, 154.43, 152.96, 152.01, 149.93, 140.63, 138.35, 136.03, 136.00, 129.24, 129.08, 122.00, 120.91, 118.95, 118.77, 117.28, 116.69, 98.29, 87.34, 20.28, 18.94

Biological Screening

In vitro anti-tubercular activity

Newly synthesized 7-hydroxy-5-methyl-N- substituted phenyl-2-(substituted phenylamino)pyrazolo[1,5-*a*]pyrimidine-3-carboxamide (6a-6i) derivatives were screened for *in-vivo* anti-mycobacterial activity against H37Rv strain using Micro plate Alamar Blue Assay method (Niu et al., 2013). Streptomycin, Pyrazinamide, and Ciprofloxacin were used as standard drugs. This methodology is non-toxic, uses thermally stable reagents and showed

good correlation with the proportional and BACTEC radiometric method. To minimize evaporation of medium from wells during incubation sterile deionized water was added to all outer perimeter of 96 wells plate. To that 100 μL of the Middle Brook 7H9 broth and serial dilutions of final drug concentrations tested were 100 to 0.2 μg/mL and incubated at 37ºC for five days. To this freshly prepared mixture of 25μL Alamar Blue reagent and 10% tween 80 was added and again incubated for 24 hrs. A blue color in the well was inferred as no bacterial growth, pink color was recorded as growth and MIC defined as lowest concentration which prevents color change from blue to pink.

MDR-TB and XDR-TB study

Potent compounds **6b, 6d** and **6h** from *in vitro* anti-tubercular screening method further opted for MDR-TB and XDR-TB study using Lowenstein-Jensen medium (L. J. medium) on H37Rv strain (Maria at al., 2007). Susceptibility of the compounds checked against multidrug-resistant TB (MDR-TB) and extensively drug-resistant TB (XDR-TB) strains. Eggs were broken aseptically and the solution was filtered through a sterile muslin cloth. To that solution 4 mL of sterilized malachite green solution is added. This mineral salt solution consist of potassium phosphate (4.0 g), magnesium sulphate (0.4 g), magnesium citrate (1.6 g), asparagine (6.0 g), glycerol (20 mL) and distilled water to make up the volume up to 1000 mL. The contents were mixed well to form a uniform medium. Synthesized targeted compounds were dissolved in 10 mL dimethyl sulfoxide (DMSO) and an aliquot 0.8 mL of each concentration was transferred into different McCartney bottles. To this, 7.2 mL of L. J. medium was added and mixed well. Isoniazid was considered as a reference standard for the comparison of anti-tubercular activity. The bottles were incubated at 75˚C - 80˚C for 3 days for solidification and sterilization.

MTT Cytotoxicity activity

Viable cells are able to reduce the yellow MTT (Tetrazolium bromide) under tetrazolium ring cleavage into a purple-blue water insoluble formazan product which precipitates in the cellular cytosol and can be dissolved after cell-lysis. Whereas cells are being dead following a toxic damage, cannot transform MTT (Stover et al., 2000). This formation production is proportionate to the viable cell number and inversely proportional to the degree of cytotoxicity. Vero Cell line was obtained from National Centre for Cell Sciences (NCCS), Pune. Anti-tuberculosis active compounds (with MIC < 12.5μg/mL) **6b, 6d** and **6h** were further evaluated for its toxicity against mammalian Vero cell line. After 72 h of exposure, viability was assessed on the basis of cellular conversion of MTT into a formazan product using the Promega Cell Titer 96 non-radioactive cell proliferation assay. These results are

important as these compounds with their increased cytoliability are much attractive in the development of new chemical entities for the treatment of TB. This is primarily due to the fact that the eradication of TB requires a lengthy course of treatment, and the need for an agent with a high margin of safety becomes a primary concern.

Results and Discussion

Pharmacophore model

Ligands with resemble conformation and selective biological activity were used to develop reliable pharmacophore model. With the information of training set molecules ten hypotheses (named as Hypo 1 to Hypo 10) were generated. The details of the generated models along with its statistical and cost values are presented in **Table 2**. Hypo 1, a four point pharmacophore model with two features (1 HBA and 3 HY) **Figure 2** showed good correlation ($r^2 = 0.85$) and low RMSD value of 1.64. The null cost (consideration of cost without any features) is 230, and fixed cost (cost of a perfect hypothesis) is 94 and configuration cost is 14.15. The greater the difference between null cost and total cost value shows the more statistically significant and reliable hypothesis (He et al., 2006). The difference between the null cost and fixed cost should be > 60 bits. It was encouraging to see that this difference is 95.26 for model Hypo 1, which signifies 90% chance of accurate correlation in the data. Configuration cost < 17 (14.15 for generated model) indicates that the generated models are not by chance correlation (He et al., 2006).

Table 2. Cost analysis and statistical characteristics of the generated pharmacophore models

Hypo No.	Features	Total cost	Δ cost	Correlation	RMS deviation
1	**HBA,HY,HY,HY**	**135.4**	**95.26**	**0.850**	**1.64**
2	HBA,HY,HY,HY	136.1	94.55	0.850	1.66
3	HBA,HY,HY,HY	137.1	93.63	0.846	1.67
4	HBA,HY,HY,HY	141.2	89.42	0.830	1.75
5	HBA,HY,HY	142.7	87.93	0.820	1.79
6	HBA,HY,HY,HY	147.5	83.15	0.800	1.87
7	HBA,HY,HY,HY	147.6	86.07	0.800	1.86
8	HBA,HY,HY,HY	147.7	82.96	0.800	1.87
9	HBA,HY,HY,HY	149.5	81.1	0.800	1.88
10	HBA,HY,HY	149.8	80.87	0.790	1.92

Null Cost: 230.641, Fixed Cost: 94.35, Configuration Cost: 14.15
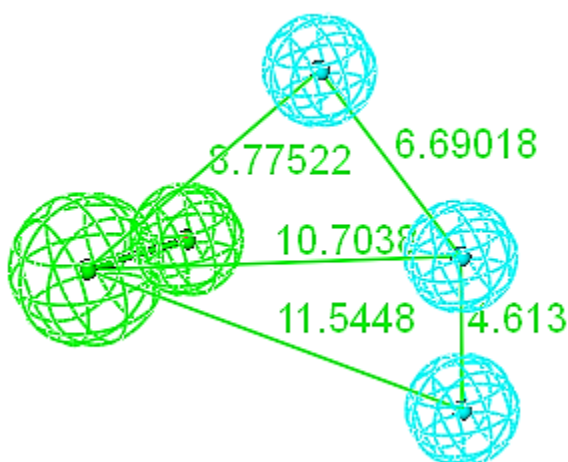
Figure 2 The common feature pharmacophore model (Hypo 1) with distance constrains. Green: Hydrogen Bond Acceptor (A), Cyan: Hydrophobic (HY).

Cross validation with test set molecules

Besides cost analysis, the generated models were further evaluated for their ability to predict the activity of test set molecules by internal and external cross validation method. The entire test set (*) molecules were mapped on Hypo 1 shown in (Table **S1**, Supplementary information). The best pharmacophore model further validated using Fischer randomization test and leave-one-out method.

Fischer randomization

The generated pharmacophore model was cross validated to check its prediction power towards the active molecules. By using the Fischer's randomization method, experimentally observed activity of the training set molecules were randomly scrambled and further rearranged to generate the HypoGen models with previously chosen parameters when generating the original pharmacophore model. The randomization result shows that none of the generated hypothesis has higher cost value and good correlation compared to Hypo 1. This value recommends 95 % chance for the true correlation (He et al., 2006).

Leave-one-out method

Leave-one-out method is used to cross-validate the generated pharmacophore model. Here generated pharmacophore was recomputed by omitting one compound at a time from the training set (Rao et al., 2008). This method demonstrates the correlation coefficient of Hypo1 does not depend on a single individual compound. If the parallel one compound is missing then hypothesis can predict the activity appropriately. This confirms for Hypo1 the

correlation co-efficient does not depend on a single particular compound from the training set.

Database screening

The generated HypoGen model **(Hypo 1)** was employed to screen Zinc and MiniMaybridge databases by adopting feature shape query. Newer hits were identified with optimum fit values. The retrieved hits shown in **Figure 3** were extracted based on their fit value and predicted IC_{50} values. Here circles in the figure represent both individual and clubbed pyrazole and pyrimidine heterocyclic rings act as anti-tubercular potential. So, on the basis of structural modification from the virtual screening we designed newer series of clubbed pyrazolo[1,5-*a*]pyrimidine analogues as potential anti-tubercular agent.
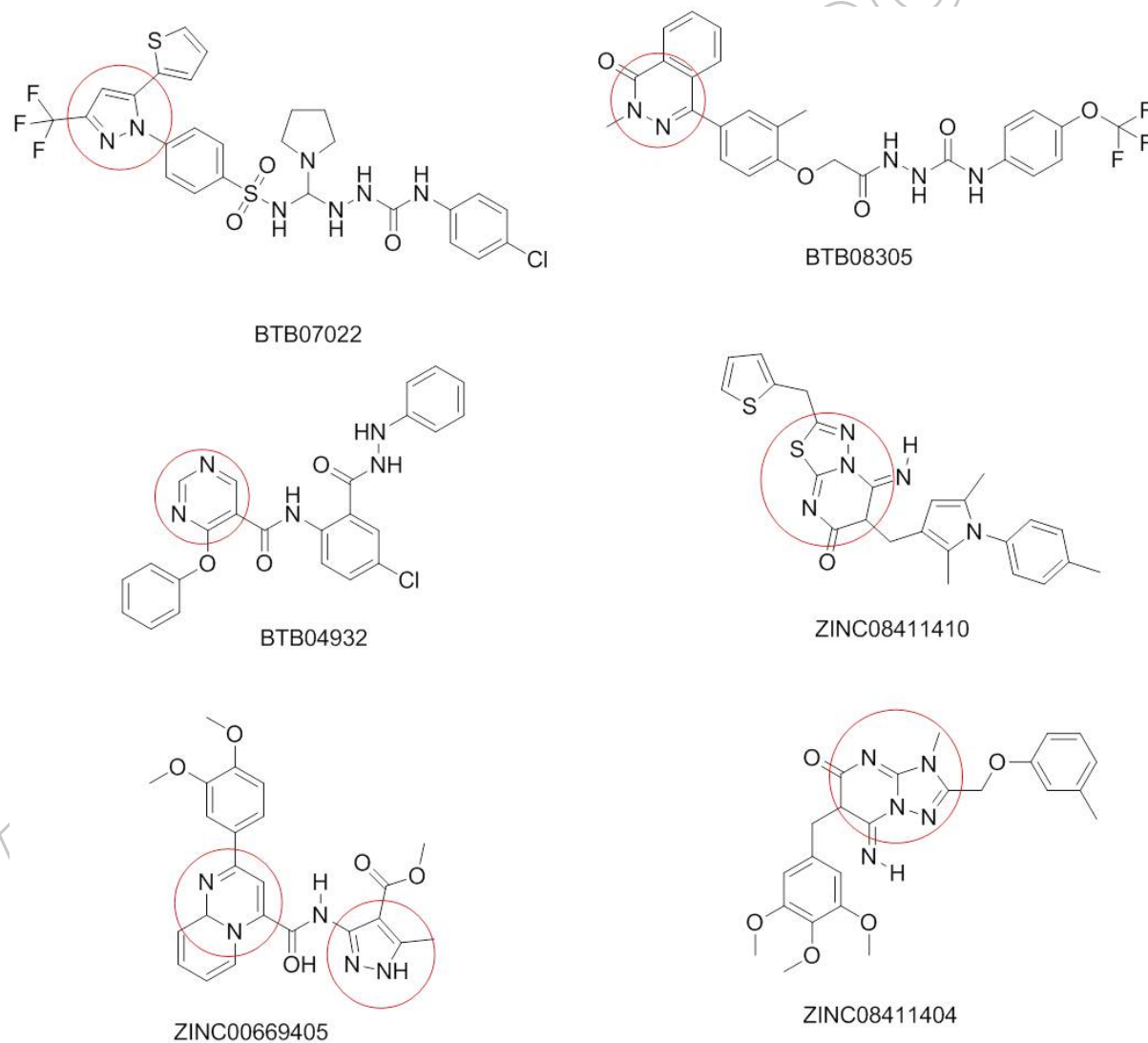
Figure 3 The retrieved hits on the basis of virtual screening of the ZINC and MiniMaybridge databases

Molecular Docking

Molecular docking is a part of the structure based drug design approach conveying knowledge of enzyme-inhibitor complex with respect to binding affinity and binding mode using Glide module of Schrodinger (Maestro v10.1, Schrodinger, LLC, NEW YORK, NY) (Sinosh et al., 2018). The cross validation of docking protocol exhibited that 2H7M protein retains the native binding interactions with lowest binding energy in comparison to other crystal structures of protein. The binding interactions of primary hits were also studied by performing docking analysis against 2H7M protein. The docking results with predicted IC_{50} values of pyrazolo[1,5-*a*]pyrimidine analogues surviving to the Lipinski's rule of five (**6a-6i**) are summarized in **Table 3**.

Table 3. Results of the database screening and docking of the identified potent compounds

Compound Name/Code	Estimated IC_{50} (µM) by Hypo 1	Glide Score
Co-Crystal ligand	2.9	-8.400
6a	0.002	-8.774
6b	0.598	-9.901
6c	0.067	-8.471
6d	0.299	-10.841
6e	0.121	-7.991
6f	0.153	-7.621
6g	0.166	-9.480
6h	0.261	-10.675
6i	0.084	-6.937

All the docked ligands occupy the identical interactions with hydrophobic cavity Met103, Phe149, Pro156 Tyr158, Met161, Met199, Ile202 and Leu218 and side chain π-π residual interaction with Phe149, Gly14 and Gly96. Also some of the compounds shows hydrogen bond network with the catalytic residue Lys165. Topmost hit molecules (**6a-6i**) amongst predicted pyrazolo[1,5-*a*]pyrimidine analogues were further synthesized and evaluated for its anti-tubercular potential.

Analysis of complexes

Amongst all synthesised analogues we have selected some of the most potent inhibitors **6b, 6d** and **6h** possess -9.901, -10.841 and -10.675 docking score and MIC 3.12, 0.8 and 0.8 µg/ml respectively which has been discussed in detail below. Compound 2-((3-chloro-4-fluorophenyl)amino)-7-hydroxy-N-(4-methoxyphenyl)-5-methylpyrazolo[1,5-a]pyrimidine-3-carboxamide **(6b) Figure 4(a)** phenyl ring showed hydrogen bonding interaction with Lys165 and hydrophobic interaction with important key amino acid residues Ile21, Met103, Met147, Phe149, Pro156, Tyr158, Met199, Ile 202 and Leu218 which indicates the summary of all the forces interacted between the ligands and InhA enzyme. Hydrogen bonds are important performers and responsible for its specificity towards targeted enzyme [28]. Here two water molecules takes part for hydrogen bonding which increases the ligand binding affinity towards the protein. The compound 2-((3-chlorophenyl)amino)-7-hydroxy-N-(4-methoxyphenyl)-5-methylpyrazolo[1,5-a]pyrimidine-3-carboxamide **(6d) Figure 4(b)** also suggest hydrogen bond interaction through oxygen with Lys165 and major important hydrophobic interacting residues are Ile21, Met103, Met147, Phe149, Pro156, Tyr158, Lys165, Ile194, Met199, Leu218, Ile202 and Ile215. Also compounds 5-amino-N-(2,4-dimethylphenyl)-3-((2-methoxyphenyl)amino)-1H-pyrazole-4-carboxamide **(6h) Figure 4(c)** have molecular interactions with Ile21, Met103, Met147, Phe149, Tyr158, Pro156, Lys 165, Ala191, Ile194, Ile202, Leu218 also one water molecule incorporating which indicates same residue comparing to co-crystalline structure which could be further potent novel *M. tuberculosis* inhibitor. These findings suggest that the newly designed compounds may be considered as potential targets for anti-tubercular drug discovery.
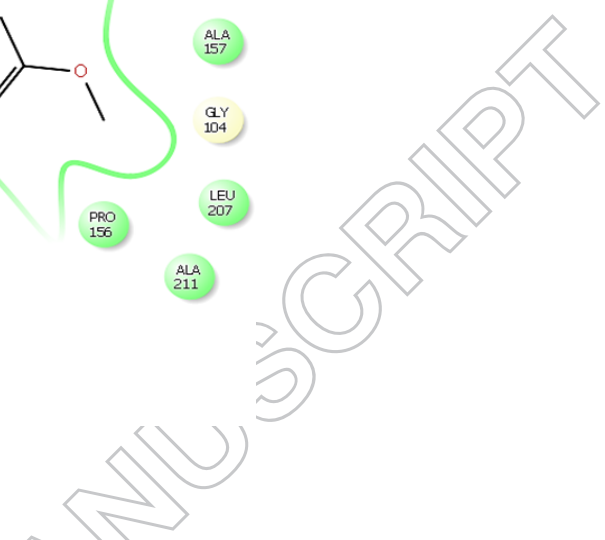
Fig. 4(a)
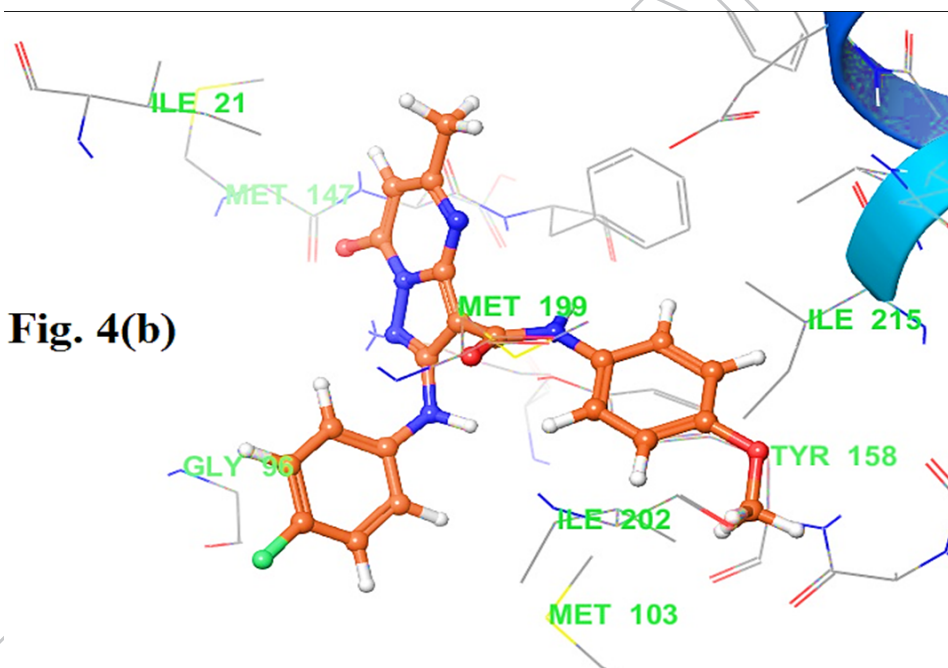
Fig. 4(b)
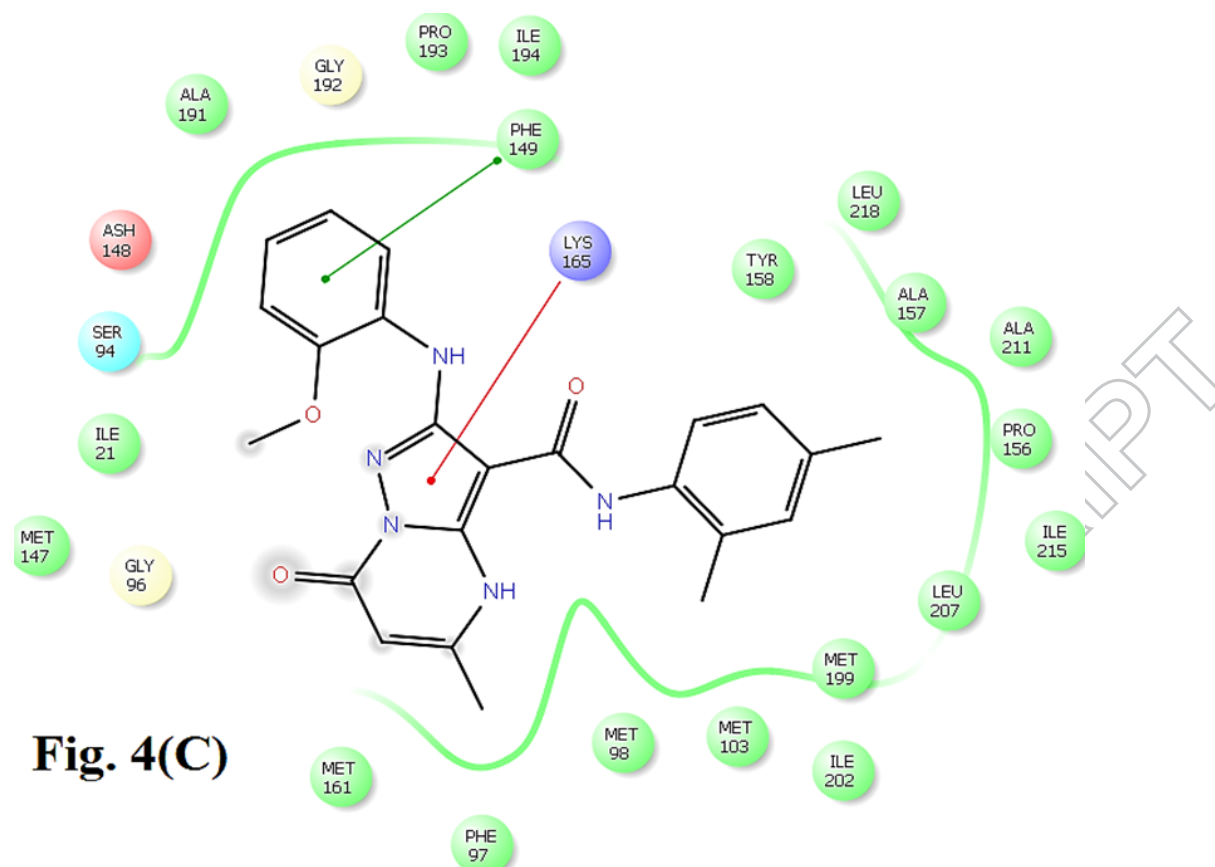
Figure 4 Docking conformation of the most potent inhibitors (a) **6b,** (b) **6d** and (c) **6h** with binding pocket of InhA enzyme (PDB : 2H7M)

In-silico **ADME prediction:**

Good efficiency with an acceptable ADMET profile is the important criteria for the accomplishment of a drug. The identified potential leads of Pyrazolo[1,5-*a*]pyrimidine derivatives **(6a-6i)** through molecular docking study were further screened for *in-silico* ADMET prediction to check its druggability using QikProp module in Schrodinger. This predicts several significant physical descriptors like molecular weight, octanol/water partition coefficient, aqueous solubility, QPPcaco for cell permeability, brain/blood partition coefficient, QPlogHERG for blockage of HERG K+ channels, metab for number of metabolic reactions, QPlogKhsa for Prediction of binding affinity to human serum albumin and percentage human oral absorption and mutagenicity compared to the properties of a particular known drugs. The results are shown in **Table 4**. Small molecules that comply with Lipinski's rule of five were further opted for the synthesis.

Table 4. ADMET properties of synthesized compounds (6a-6i)

Comp.	MW	Log P o/w	Log S	QPP Caco	Log BB	QPlog HERG	Metab	QPLog Khsa	% Oral abs
6a	407.11	4.684	-6.802	1359.021	-0.68	-6.995	6	0.539	100
6b	441.10	4.433	-6.75	1005.631	-0.76	-6.986	5	0.562	100
6c	407.14	4.13	-6.193	1004.219	-0.57	-7.004	6	0.468	100
6d	423.11	4.364	-6.561	1004.788	-0.51	-6.939	6	0.404	100
6e	411.09	4.261	-6.383	1196.565	-.1.82	-7.032	6	0.288	100
6f	389.15	4.178	-6.335	1361.929	-0.39	-7.012	5	0.438	100
6g	395.12	3.876	-5.779	1005.099	-0.91	-6.893	6	0.328	100
6h	417.18	3.876	-5.833	1359.021	-0.77	-7.025	5	0.398	100
6i	445.02	4.493	-6.75	1005.631	-0.52	-7.028	6	0.536	100

Molecular weight (MW)-acceptable limit is <500 Da; Log P-predicted octanol/water partition coefficient with range-(2.0 to 6.5); Log S-estimated solubility limit is value greater than -4; QPPcaco-predicts Caco-2 cell permeability model for the gut-blood barrier in nm/s, where limit is <25 is considered poor and >500 is considered excellent; QPlogHERG-Predictes IC_{50} value for blockage of HERG K+ channels range (>-5); metab-Number of likely metabolic reactions range (1-8); QPlogKhsa-Prediction of binding to human serum albumin. Range (– 1.5 to 1.5); Percentage human oral absorption-this gives the predicted human oral absorption on 0-100% scale.

Chemistry

The synthetic approach for the derivatives of 7-hydroxy-5-methyl-N- substituted phenyl-2-(substituted phenylamino)pyrazolo[1,5-a]pyrimidine-3-carboxamide **(6a-6i)** is summarised in the synthetic **scheme 1**. Nucleophilic addition reaction occurs between different substituted amines and ethyl cyano acetate **(1)** for the synthesis of 2-cyano-*N*-(substitutedphenyl)acetamide **(2a-2f)**. Further protonation of the carbonyl carbon of 2-cyano-*N*-(substitutedphenyl)acetamide **(2a-2f)** will occur and undergo for nucleophilic addition reaction with the help of carbon disulphide and dimethyl sulphate to form the S, S acetal

(Ketals) derivatives **(3a-3f)**. These acetal derivatives **(3a-3f)** reacts different substituted amines for the formation of Keten S, N- acetal **(4a-4i)**. Further this S, N- acetal **(4a-4i)** will undergo for ring closure strategy with the help of hydrazine hydrate for the formation of 5-amino-N-substituted phenyl-3-(substituted phenylamino)-1H-pyrazole-4-carboxamide **(5a-5i)**. Again these pyrazole derivatives **(5a-5i)** condensed with ethyl aceto acetate to from final product 7-hydroxy-5-methyl-N- substituted phenyl-2-(substituted phenylamino)pyrazolo[1,5-*a*]pyrimidine-3-carboxamide **(6a-6i)**. All the synthesised final compounds (6a-6i) were purified and confirmed with IR, MASS, ^{1}HNMR, ^{13}CNMR spectroscopy. The IR spectrum of final compounds shows strong -OH stretching appear near to 3400 cm^{-1} and amidic carbonyl stretching at 1660 cm^{-1} which is absent in intermediate (5a-5i). Here appearance of OH group broadening in the IR spectrum confirms the formation of the condensed final pyrazolo[1,5-*a*]pyrimidine. The ^{1}H spectrum of intermediate compound (5a-5i) displays absence of the aromatic OH proton peak which is present in the final compounds nearer to δ 11.3 which confirms the formation of final cyclization product.

2a, R=4-OCH$_3$-C$_6$H
2b, R=2,4-CH$_3$-C$_6$H$_4$
2c, R=-H-C$_6$H$_6$
2d, R=4-F-C$_6$H$_6$
2e, R=3-Cl, 4-F-C$_6$H$_4$
2f, R=3-Cl-C$_6$H$_5$

6a, R=3-Cl-C$_6$H$_5$,   R'=4-CH$_3$-C$_6$H$_5$
6b, R=4-OCH$_3$-C$_6$H$_5$, R'=3-Cl, 4-F-C$_6$H$_4$
6c, R=4-OCH$_3$-C$_6$H$_5$, R'=4-F-C$_6$H$_5$
6d, R=4-OCH$_3$-C$_6$H$_5$, R'=3-Cl-C$_6$H$_5$
6e, R=-C$_6$H$_5$,   R'=3-Cl, 4-F-C$_6$H$_4$
6f, R=-C$_6$H$_5$,   R'=4-OCH$_3$-C$_6$H$_5$
6g, R=4-F-C$_6$H$_5$,   R'=4-F-C$_6$H$_5$
6h, R=2,4-CH$_3$-C$_6$H$_4$, R'=2-OCH$_3$-C$_6$H$_5$
6i, R=3-Cl, 4-F-C$_6$H$_4$, R'=3-Cl-C$_6$H$_5$
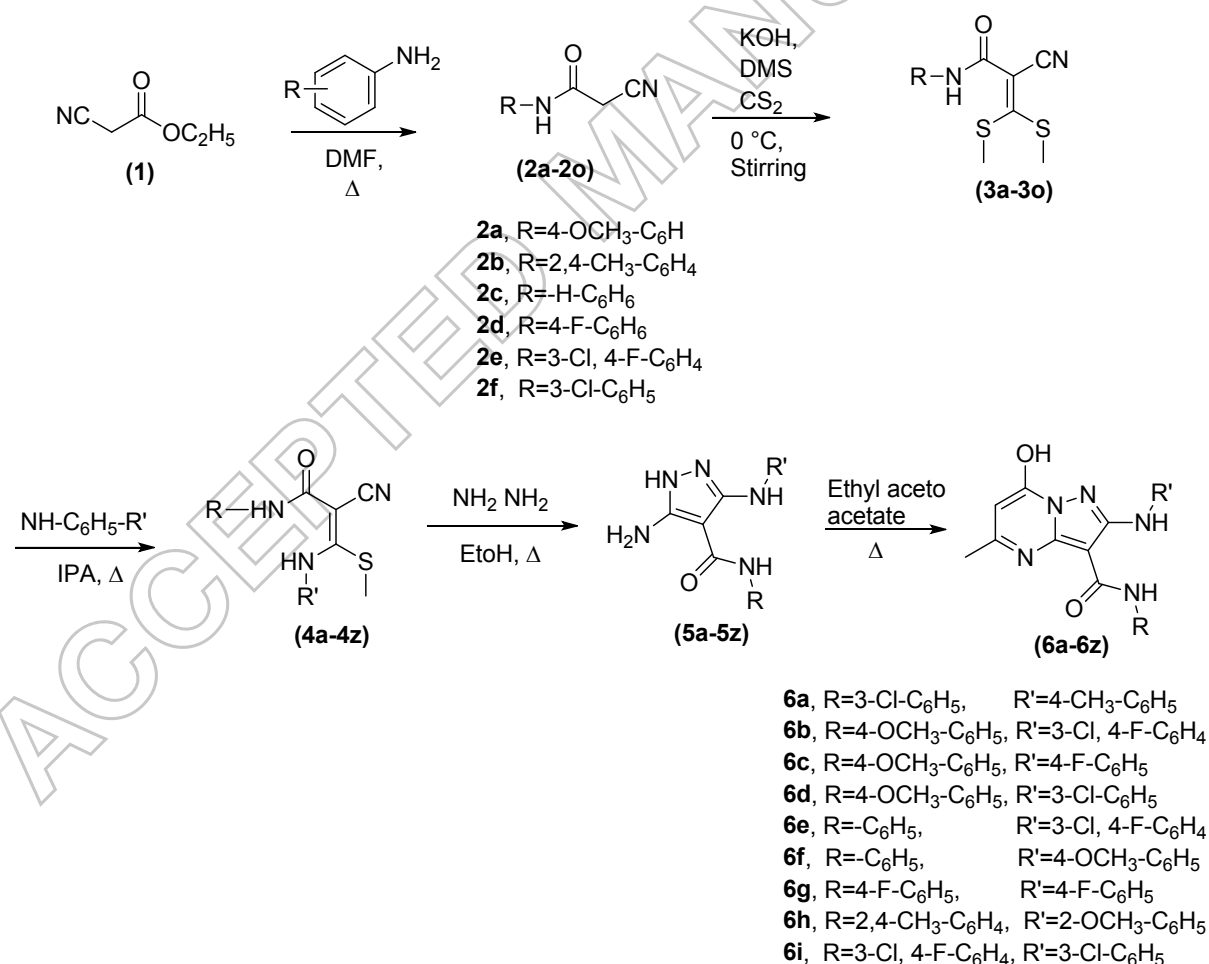
Scheme 1 synthetic approach for the derivatives of 7-hydroxy-5-methyl-N- substituted phenyl-2-(substituted phenylamino)pyrazolo[1,5-*a*]pyrimidine-3-carboxamide (6a-6i)

Anti-tubercular studies

Newer series of pyrazolo[1,5-*a*]pyrimidine **(6a-6i)** derivatives were synthesized and evaluated for its anti-tubercular potential against *Mycobacterium tuberculosis* H37Rv strain by Micro plate Alamar Blue Assay (MABA) method. All the synthesized compounds possess good to moderate inhibitory activity compared to standard drugs Pyrazinamide, Ciprofloxacin and streptomycin. *In vitro* anti-tubercular activity with MIC levels of the titled compounds **(6a–6i)** are presented in **Table 5**. Amongst screened all the synthesized compounds **6d** (R= 4-OCH$_3$, R'= 3-Cl) and **6h** (R= 2,4-CH$_3$, R'= 2-OCH$_3$) demonstrates an excellent activity against *M. tuberculosis* with MIC of 0.8 µg/mL. Also one of the compound **6b** (R= 4-OCH$_3$, R'= 3-Cl 4-F) have shown MIC 3.12 µg/mL which is as active as standard drug Pyrazinamide and Ciprofloxacin. One of the compound **6g** (R= 4-F, R'= 4-F) showed MIC 6.25 µg/mL, as potent as standard drug streptomycin. However compounds **6a** (R= 3-Cl, R'= 4-CH$_3$)**, 6c** (R= 4-OCH$_3$, R'= 4-F) and **6f** (R= NH, R'= 4-OCH$_3$) exhibited good anti-tubercular activity with MIC 12.5 µg/mL but starting to loss the potency. Other remaining compounds **6e** (R= -NH, R'= 3-Cl 4-F) and **6i** (R= 3-Cl 4-F, R'= 3-Cl) possess anti-tubercular activity with MIC 25 µg/mL. Identified newer potent compounds **6b, 6d** and **6h** further opted for MDR-TB, XDR-TB and cytotoxicity study.

Table 5. Anti-mycobacteraial activity of pyrrazolo[1,5-*a*]pyrimidine (6a-6i)

Sample code	R	R'	MIC(µg/ml)
6a	3-Cl	4-CH$_3$	12.5
6b	4-OCH$_3$	3-Cl 4-F	3.12
6c	4-OCH$_3$	4-F	12.5
6d	4-OCH$_3$	3-Cl	0.8
6e	NH	3-Cl	25
6f	NH	4-OCH$_3$	12.5
6g	4-F	4-F	6.25
6h	2,4-CH$_3$	2-OCH$_3$	0.8
6i	3-Cl 4-F	3-Cl	25
	Pyrazinamide		3.12
	Ciprofloxacin		3.12
	Streptomycin		6.25

MDR-TB and XDR-TB

From the Synthesized newer designed analogues some of the compounds **6b, 6d** and **6h** demonstrate the potent anti-tubercular activity against *M. tuberculosis* H37Rv strain via MABA method. Further they were assayed by Lowenstein-Jensen medium (L.J. medium) to check their susceptibility against multidrug resistant Tb (MRD-TB) and extensively drug-resistant TB (XDR-TB). The results are summarized in **Table 6**.

Table 6. MDR-TB and XDR-TB strain using Lowenstein-Jensen medium and Cytotoxicity study on Vero cell line

Sr. No.	R	R'	MIC (µg/mL)			Cytotoxicity IC$_{50}$ (µg/mL)
			H37Rv	MDR-TB	XDR-TB	
6b	4-OCH$_3$	3-Cl 4-F	3.12	12.5	>100	5.4
6d	4-OCH$_3$	3-Cl	0.8	1.6	50	7.3
6h	2,4-CH$_3$	2-OCH$_3$	0.8	3.2	12.5	11.02
	Isoniazide		0.5	6.25	50	ND

ND: Not determined

IC$_{50}$ values are the mean of triplicate study

Cytotoxicity assay

The cellular transformation of MTT [3-(4,5-dimethylthiazo-2-yl)-2,5-diphenyl-tetrazolium bromide] is a pale yellow substrate which converted into a formazan a dark blue product, computed by colorimetric methods. Some of the selected potent anti-tubercular compounds of **6b, 6d** and **6h** were further evaluated for cytotoxic activity against a mammalian Vero cell followed by the determination of IC$_{50}$ **Table 6**. Among all the synthesized compounds **6b** has lowest IC$_{50}$ 5.4 µg/mL on mammalian VERO cell line. Also, compounds **6d** and **6h** shows effect on cancer cell line with IC$_{50}$ values around 7.3 µg/mL and 11.2 µg/mL respectively.

Conclusion

With the emergence of MDR-TB, XDR-TB and recent cases of TDR-TB, discovery of newer anti-tubercular drug is currently driving the resurgence. Enoyl acyl carrier protein (ACP) reductase plays critical role in the biosynthesis of mycobacterial cell wall, which is the promising target for tuberculosis. In the present work, we have designed and synthesized a series of 7-hydroxy-5-methyl-*N*- substituted phenyl-2-(substitutedphenylamino)pyrazolo[1,5-

a]pyrimidine-3-carboxamide (6a-6i) derivatives via pharmacophore-based virtual screening and molecular docking studies. This studies also suggests compounds **6b, 6d** and **6h** interacted more efficiently with InhA enzyme. Looking at the bioactivity of final potent nucleus, the synthesized derivatives **6b, 6d** and **6h** showed potent anti-tuberculosis activities which were found to be comparable to the reference standard drugs with less toxicity. The potent assumption opens up new potential targeted molecules where discovery will yield novel anti-tuberculosis agents.

Acknowledgments

The authors acknowledge Oxygen healthcare, Changodar and Saurashtra University, Rajkot for providing analytical instrumental data and Maratha Mandal's NGH Institute of Dental Sciences and Research Centre, Belguam, Karnataka, India for biological screening facilities.

Conflicts of interest

The authors declare no conflict of interest about this article.

Supporting Information

The training and test set molecules to generate the pharmacophore models as well ¹H NMR and ¹³C NMR spectra have been provided for all the final compounds.

References
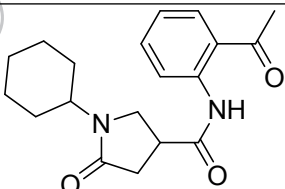
Asselineau, J., Lederer, E. (1950). Structure of the Mycolic acid of Mycobacteria. *Nature*, 166, 782-783.

Banerjee, A., Dabnau, E., Quemard, A., Balasubramanian, V., Um, K. S., Wilson, T., Collins, D., De, L. G., Jacobs, W. R. (1994). InhA, a gene encoding a target for isoniazid and ethionamide in Mycobacterium tuberculosis. *Science*, 263, 227-230.

Dye, C., Lonnroth, K., Jaramilo, E., Williams, B. G., Raviglione, M. (2009). Trends in tuberculosis incidence and their determinants in 134 countries. *Bull. World Health Organ*, 87, 683-691.

Funk, O. F., Kettmann, V., Drimal, J., Langer, T. (2004). Chemical Function Based Pharmacophore Generation of Endothelin-A Selective Receptor Antagonists. *J Med Chem*, 47, 2750-2760.

Halgren, A., Murphy, B., Friesner, R. A., Beard, H. S., Frye, L. L., Pollard, W. T., Banks, J. L. (2004). Glide: A new approach for rapid, accurate docking and scoring 2. Enrichment factors in database screening. *J Med Chem*, 47, 1750-1759.

He, X., Alion, A., Ortiz, D. E., Montellano, P. R. (2007). Inhibition of the *Mycobacterium tuberculosis* enoyl acyl carrier protein reductase InhA by arylamides. *Bioorg Med Chem.*, 15, 6649-6658.

He, X., Allian, A., Stroud, R., Ortiz, D. E., Montellano, P. R. (2006). Pyrrolidine carboxamides as a novel class of inhibitors of enoyl acyl carrier protein reductase from Mycobacterium tuberculosis. *J Med Chem.*, 49, 6308-6323.

Irwin, J., Sterling, T., Mysinger, M., Bostand, S., Coleman, G. (2012). ZINC: A free tool to discover chemistry for biology. *J of Chem Info & Modelling*, 52, 1757-1768.

Maria, C. S., Marcus, V. N., DeSouza, A. C. P., Marcelle, D. L., Rasnisb, B., Cristina, M., Nogneira, M., Peralta, A. (2007). Evaluation of anti-Tubercular activity of nicotinic and isoniazid analogues. *ARKIVOC*, 15, 181-191.

Maestro v10.1 (2009) Glide, Schrodinger, LLC, New York.

Mason, J. S., Good, A. C., Martin, E. J. (2001). 3D pharmacophore in Drug discovery. *Curr Pharm Des.*, 7, 567-597.

Mohsin, Y. L., Mohd., A., Vivek, K. G., Prakash, C. J. (2017). Identification of Mycobacterium tuberculosis enoyl-acyl carrier proteinreductase inhibitors: A combined in-silico and in-vitro analysis. *J Mol Graph Model.*, 76, 172–180.

Mohsin, Y. L., Anu M., Mohd. A., Prakash, C. J. (2017). Identification of InhA inhibitors: A

combination of virtual screening, molecular dynamics simulations and quantum chemical studies. *J Biomol Struct Dyn.,* DOI:10.1080/07391102.2017.1372313.

Niu, M., Dong, F., Tang, S., Fida, G., Qin, J., Qui, J., Liu, K., Gao, W., Gu, Y. (2013). Pharmacophore Modeling and Virtual Screening for the Discovery of New type 4 cAMP Phosphodiesterase (PDE4) Inhibitors. *PLOS ONE*, 8(12), e82360.

Podlogar, B. L., Ferguson, D. M. (2000). QSAR and CoMFA: a perspective on the practical application to drug discovery. *Drug Des Discov*, 17, 4-12.

Quemard, A., Blanchard, J. S., Jacobs, W. R., Sacchetini, J. C. (1995). Crystal structure and function of the isoniazid target of Mycobacterium tuberculosis. *Science*, 267, 1638-1641.

Rao, G. S., Vijaykrishnan, R., Kumar, M. (2008). Structure based design of novel classof potent inhibitors of InhA, the enoyl acyl carrier protein reductase from Mycobacterium tuberculosis: A Computer modelling approach. *Chem. Biol. Drug. Des.,* 72, 444-449.

Santo, D., Fermeglia, M., Ferrone, M. (2005). Simple but Highly Effective Three-Dimensional Chemical-Feature-Based Pharmacophore Model for Diketo Acid Derivatives as Hepatitis C Virus RNA-Dependent RNA Polymerase Inhibitors. *J Med Chem*, 48, 6304-6314.

Shalini, S., Maaged, A., Dharmarajan, S., Lalitha, G. (2017). Discovery of novel inhibitors of Mycobacterium tuberculosis MurG: homology modelling, structure based pharmacophore, molecular docking, and molecular dynamics simulations. *J Biomol Struct Dyn.,*DOI: 10.1080/07391102.2017.1384398.

Sinosh, S., Meghna, M., Nikhil, B. (2018). Screening of potential lead molecules against prioritised targets of multi-drug-resistant-Acinetobacter baumannii – insights from molecular docking, molecular dynamic simulations and in vitro assays. *J Biomol Struct Dyn.,* DOI: 10.1080/07391102.2018.1451387.

Sivakumar, P. M., Seenivasan, S. P., Kumar, V., Doble, M. (2007). Synthesis, antimycobacterial activity evaluation, and QSAR studies of chalcone derivatives. *Bioorg Med Chem Lett*, 17, 1695-1700.

Stover, C.K., Warrener, P., Van Devanter, D.R., Sherman, D.R., Arain, T.M., Langhorne, M.H. and Anderson, S.W. (2000). A Small-Molecule Nitroimidazopyran Drug Candidate for the Treatment of Tuberculosis. *Nature*, 405, 962-966.

Takayama, K., Wang, C., Besra, G. S. (2005). Pathway to synthesis and processing of mycolic acids in Mycobacterium tuberculosis. *Clin Microbil Rev*, 18, 81-101.

Tsukamura, M., Wang, C., Besra, S. (1978). A comparison of the time of *in vivo* resistance development of tubercle bacilli to Rifampicin, Kanamycin, Ethionamide, Lividomycin, and Enviomycin (Tuberactinomycin-N) in patients with chronic cavitary Tuberculosis. *Kekkaku (Tuberculosis)*, 53, 495-498.

Williams, P., Floyd, K., Dye, C., Elzinga, G., Raviglione, M. (2005). Tuberculosis control in the era of HIV. *Nat. Rev. Immunol*, 5, 819-826.

Yang, Y., Xu, S., Zhang, M., Jin, R., Zhang, L., Bao, J., Wang, H. (2006). Purification and characterization of a functionally active Mycobacterium tuberculosis pyrroline-5-carboxylate reductase. *Protein Expr Purif*, 45, 241-248.

Zhang, Y., Garbe, T., Young, D. (1993). Transformation with *katG* restores isoniazid-sensitivity in *Mycobacterium tuberculosis* isolates resistant to a range of drug concentrations. *Mol Microbiology*, 3, 521-524.

Zhang, Y., Heym, B., Allen, B., Young, D., Cole, S. (1992). The catalase-peroxidase gene and isoniazid resistance of Mycobacterium tuberculosis. *Nature*, 283, 591593.

Zhao, X., Yu, H., Yu, S., Wang, F., Sacchettini, J. C., Magliozzo, R. S. (2005). Hydrogen Peroxide-Mediated Isoniazid Activation Catalyzed by *Mycobacterium tuberculosis* Catalase−Peroxidase (KatG) and Its S315T. *Mutant Biochemistry*, 45, 4131-4140.

Supplementary material

Table S1 Structures of the training and test set of molecules and their residual values

Compd.	Chemical Structures	IC$_{50}$ (μM)	Predicted Activity	Residual
1		34.88	42.84	-7.96

2*

| 0.89 | 1.91 | -1.02 |
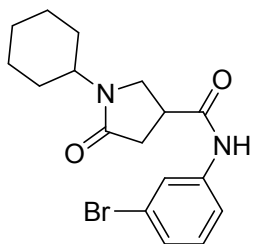
3

| 16.79 | 19.744 | -2.95 |
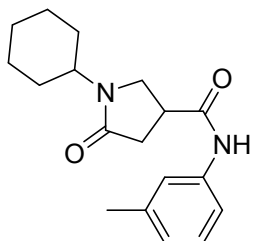
4*

| 5.55 | 9.67 | -4.12 |
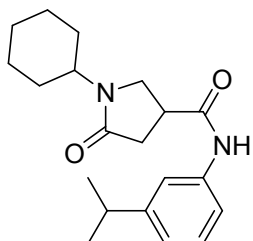
5

| 56.02 | 52.047 | 3.97 |
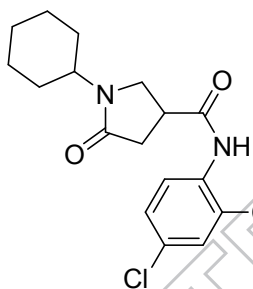
6*

| 56.5 | 45.23 | 11.27 |
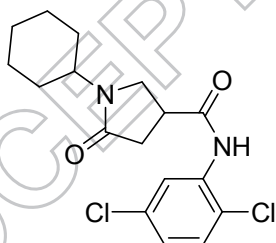
7*

| 0.97 | 5.514 | -4.54 |
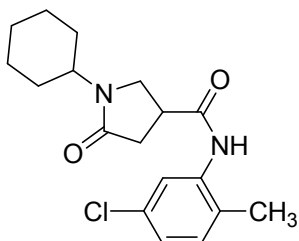
8*   37.41   32.85   4.56
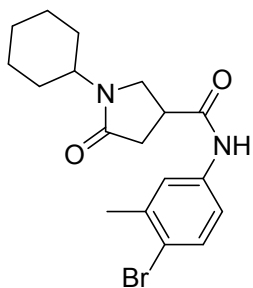
9   10.05   5.032   5.09
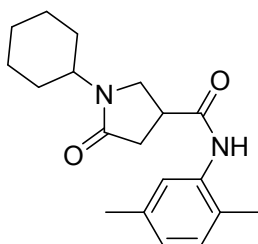
10*   23.12   25.81   -2.69
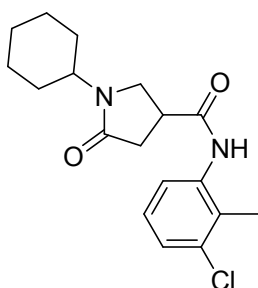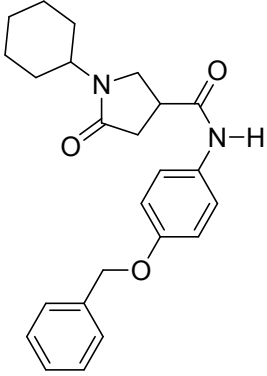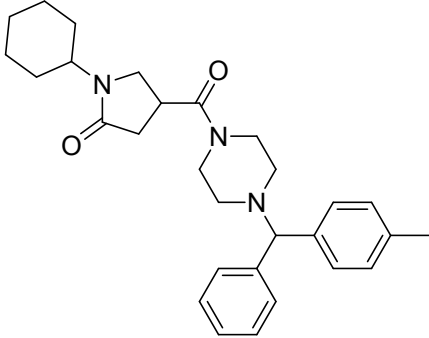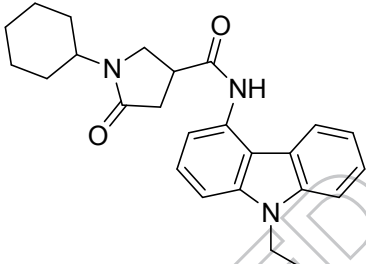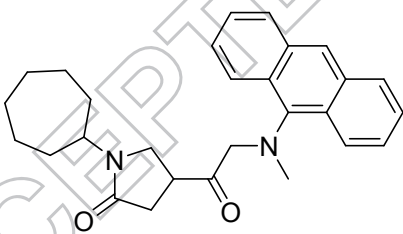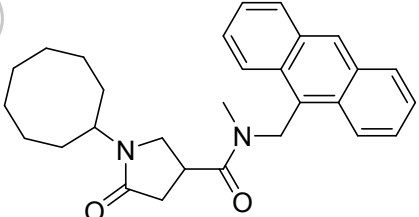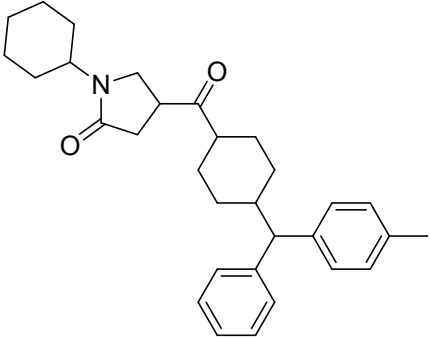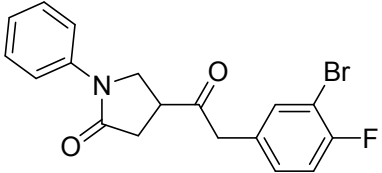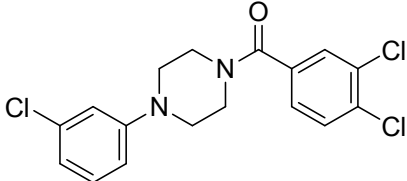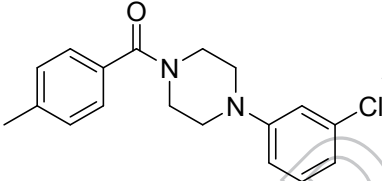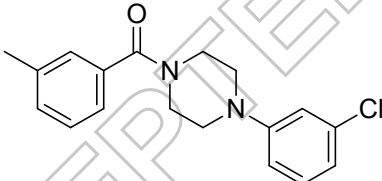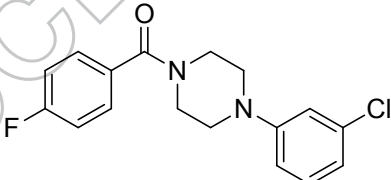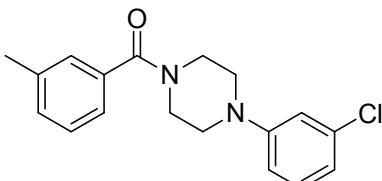
11   1.6   2.44   -0.84
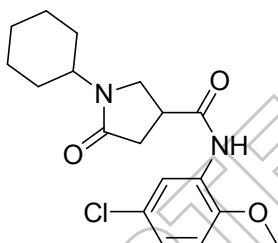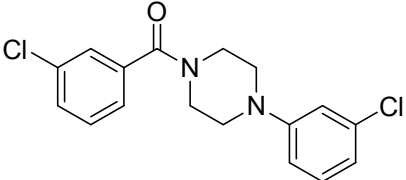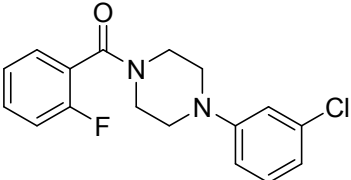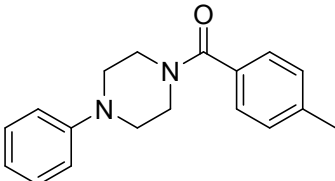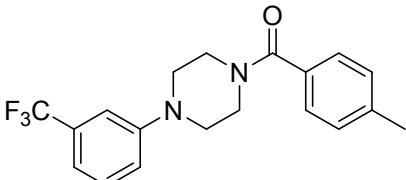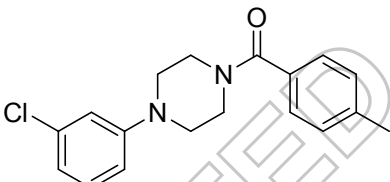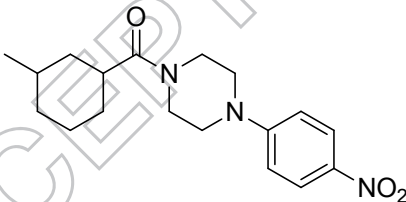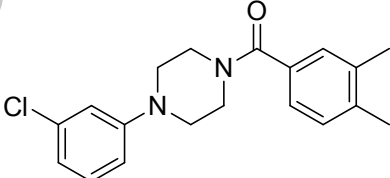
12   0.75   2.471   -1.72
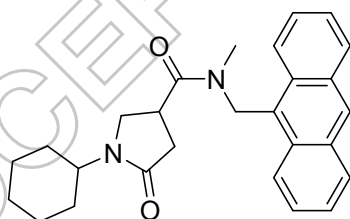
13		3.39	4.985	-1.59
14*		5.18	6.7	-1.52
15*		2.57	3.25	-0.68
16		0.62	1.44	-0.82
17		0.32	0.292	0.028

18*		2.57	0.871	1.69
19		29.23	23.161	6.07
20*		6.05	1.858	4.192
21*		3.07	4.081	-1.011
22		1.35	1.135	0.215
23		10.66	7.477	3.183
24		34.88	37.135	-2.255

25*		9.43	2.704	6.72
26*		13.87	13.55	0.32
27		16.64	18.38	-1.74
28		6.26	8.74	-2.48
29		3.07	3.509	-0.44
30		15.47	16.702	-1.23
31*		0.99	5.138	-4.418

32 F₃C ... (structure) 1.85   6.412   -4.56
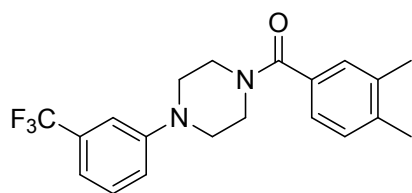
33 Cl ... (structure) 9.47   7.477   2.0

34 Cl ... Cl (structure) 6.73   2.72   4.46

35 (structure) 17.62   16.719   0.90

36 (structure) 31.5   33.02   -1.52

37 Cl ... (structure) 7.74   7.22   0.52
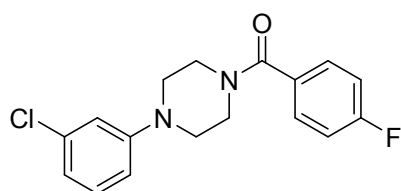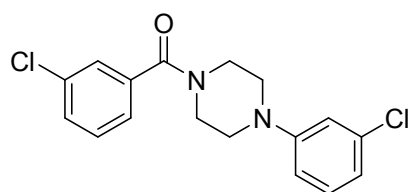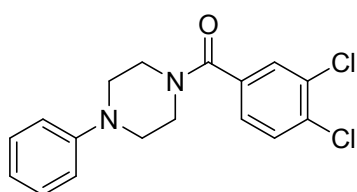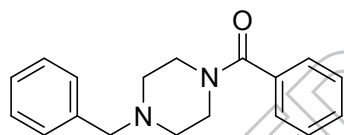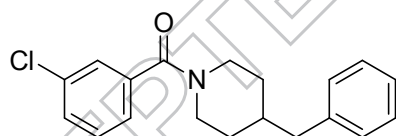
38 (structure) 1.89   1.67   0.22
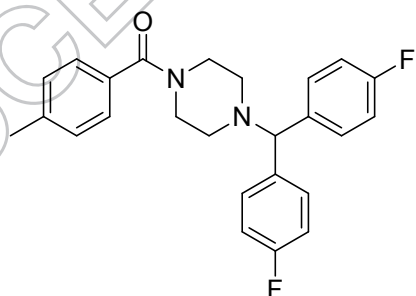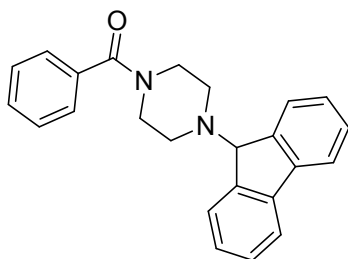
39		85.91	82.76	3.12
40		5.1	13.60	-8.5
41		0.12	0.064	0.056
42		0.46	1.029	-0.57
43		0.91	1.97	-1.06
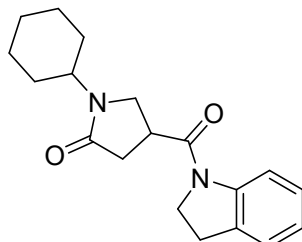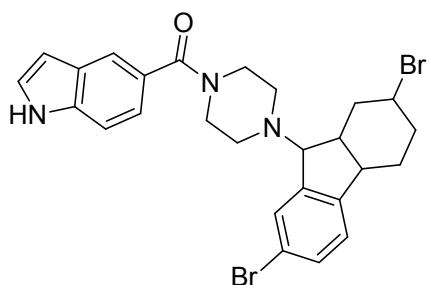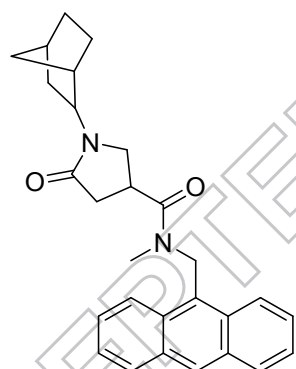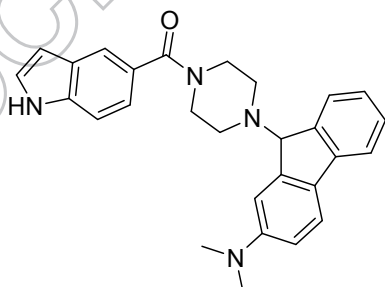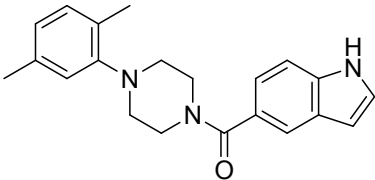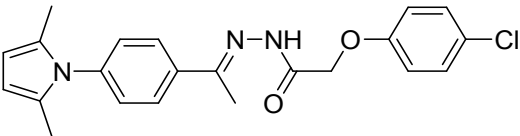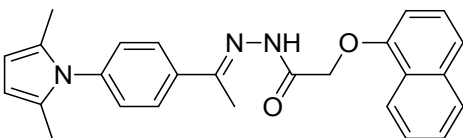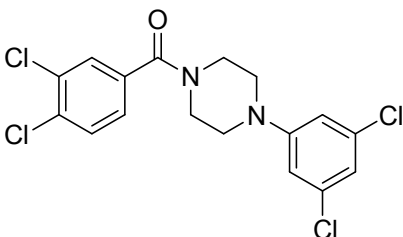
44*		1.04	1.455	-0.415
45*		3.125	0.765	2.36
46*		0.20	0.133	0.067
47		0.39	0.27	0.12

* Test set molecules

6a

Peaks (ppm): 12.039, 9.880, 8.857, 8.168, 8.148, 7.767, 7.596, 7.576, 7.409, 7.389, 7.368, 7.245, 7.169, 7.167, 7.150, 7.147, 7.117, 7.071, 7.051, 7.032, 6.990, 6.787, 6.768, 5.773, 2.502, 2.357, 2.267

Integrations: 0.84, 0.94, 1.00, 1.01, 1.02, 1.02, 1.10, 1.15, 1.02, 1.05, 1.04, 3.12, 3.12

6a

Peaks (ppm): 162.20, 154.96, 153.71, 140.18, 138.86, 136.17, 132.80, 130.22, 125.61, 123.06, 122.91, 122.70, 120.08, 119.05, 115.47, 98.33, 87.14, 40.09, 39.88, 39.67, 39.46, 39.25, 39.05, 38.84, 20.45, 12.92

6b
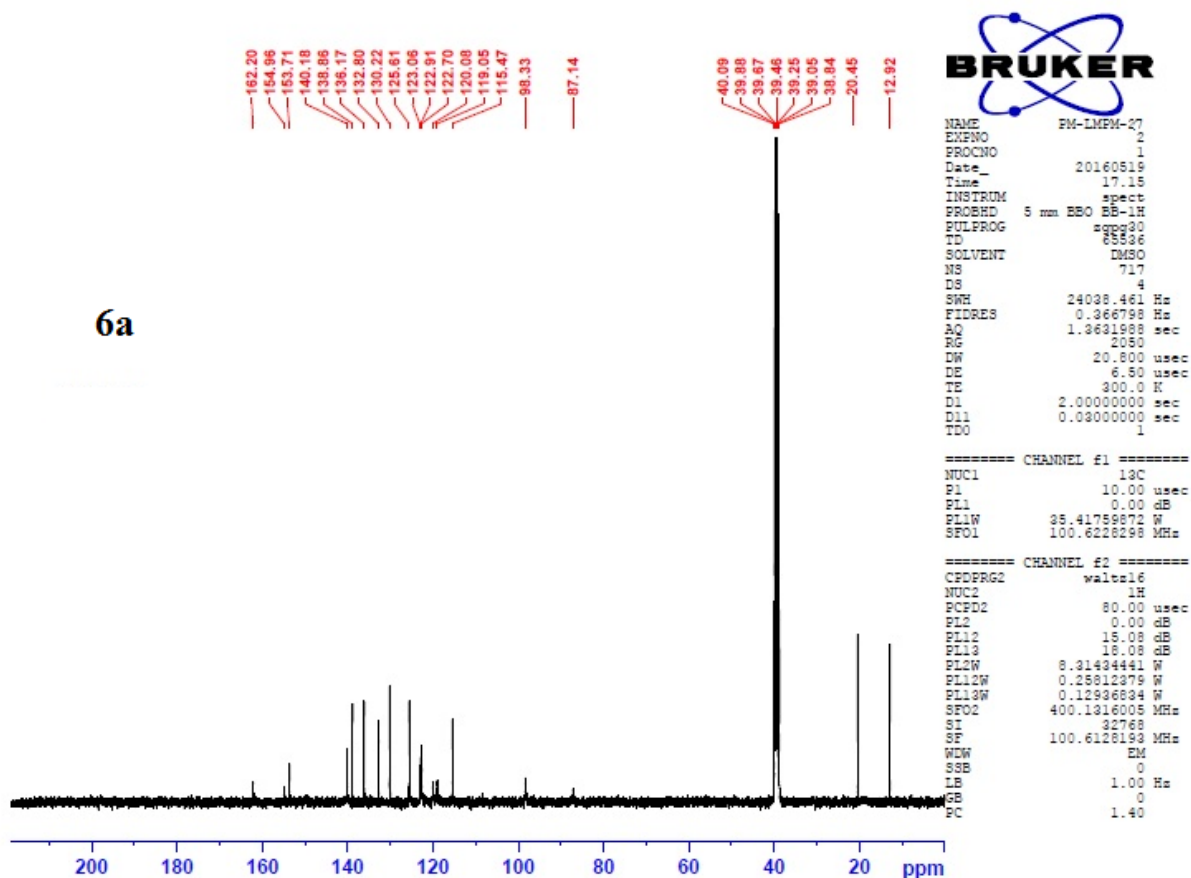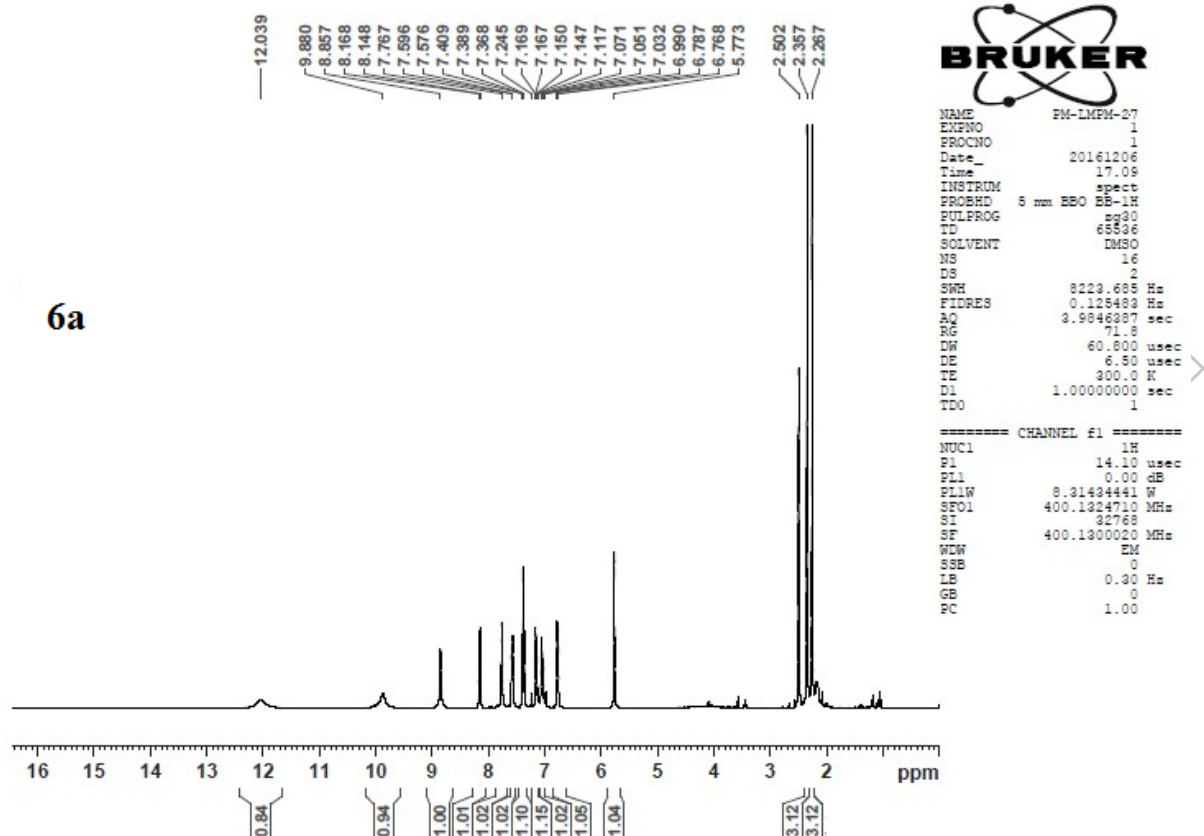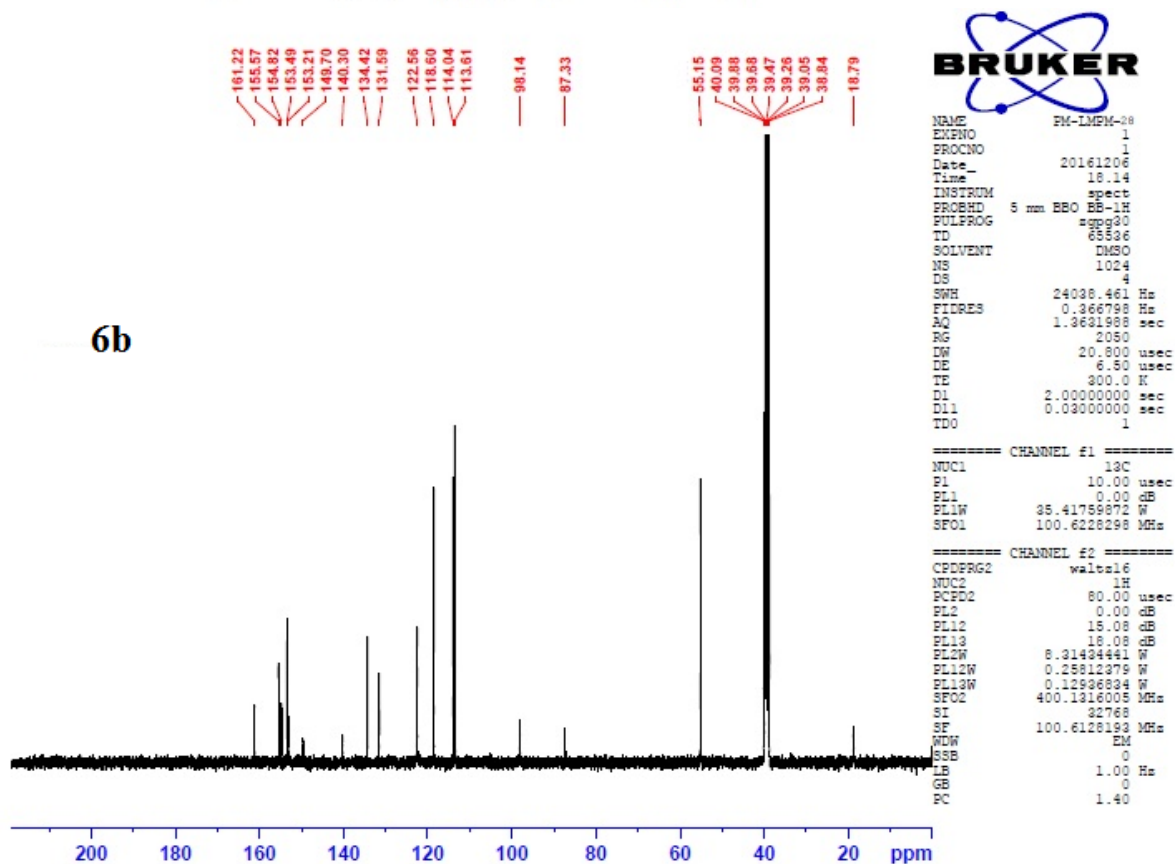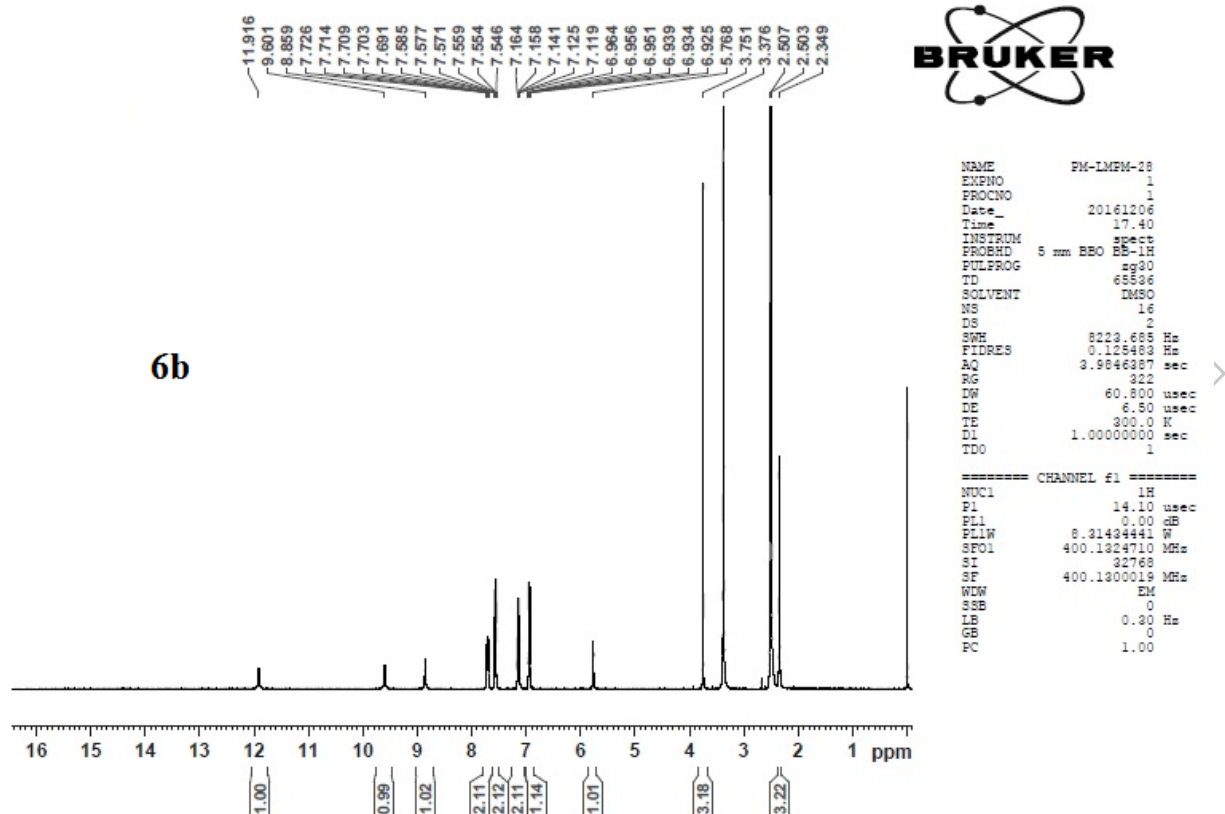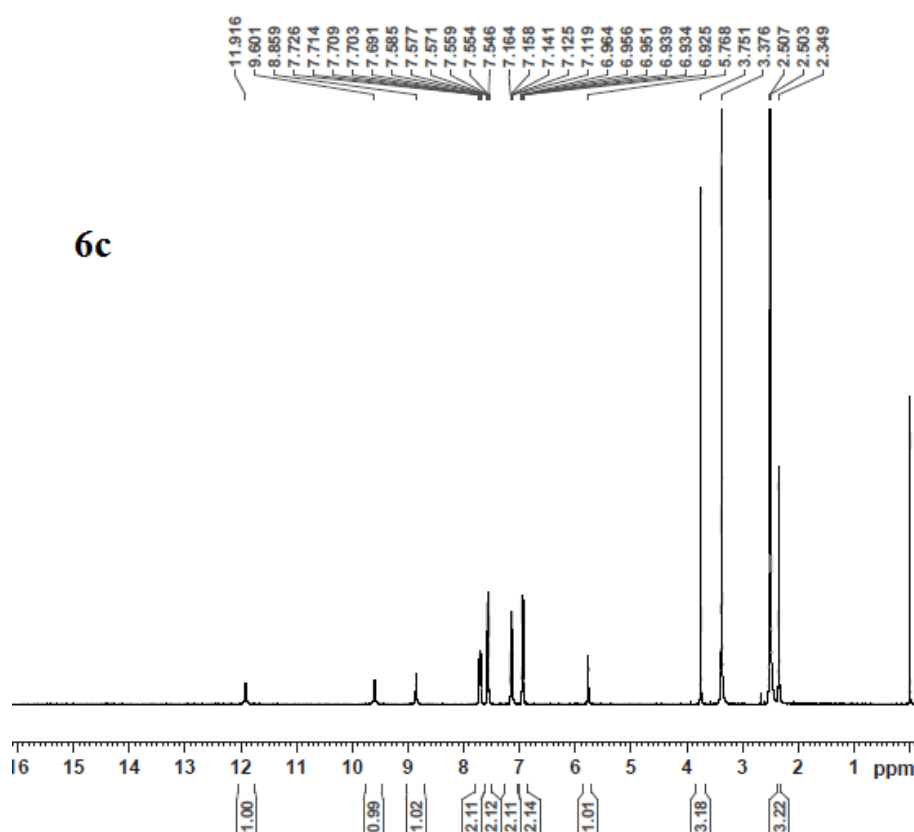
NAME   PM-LMPM-28
EXPNO   1
PROCNO   1
Date_   20161206
Time   17.40
INSTRUM   spect
PROBHD   5 mm BBO BB-1H
PULPROG   zg30
TD   65536
SOLVENT   DMSO
NS   16
DS   2
SWH   8223.685 Hz
FIDRES   0.125463 Hz
AQ   3.9846387 sec
RG   322
DW   60.800 usec
DE   6.50 usec
TE   300.0 K
D1   1.00000000 sec
TD0   1

======== CHANNEL f1 ========
NUC1   1H
P1   14.10 usec
PL1   0.00 dB
PL1W   8.31434441 W
SFO1   400.1324710 MHz
SI   32768
SF   400.1300019 MHz
WDW   EM
SSB   0
LB   0.30 Hz
GB   0
PC   1.00

6b

NAME   PM-LMPM-28
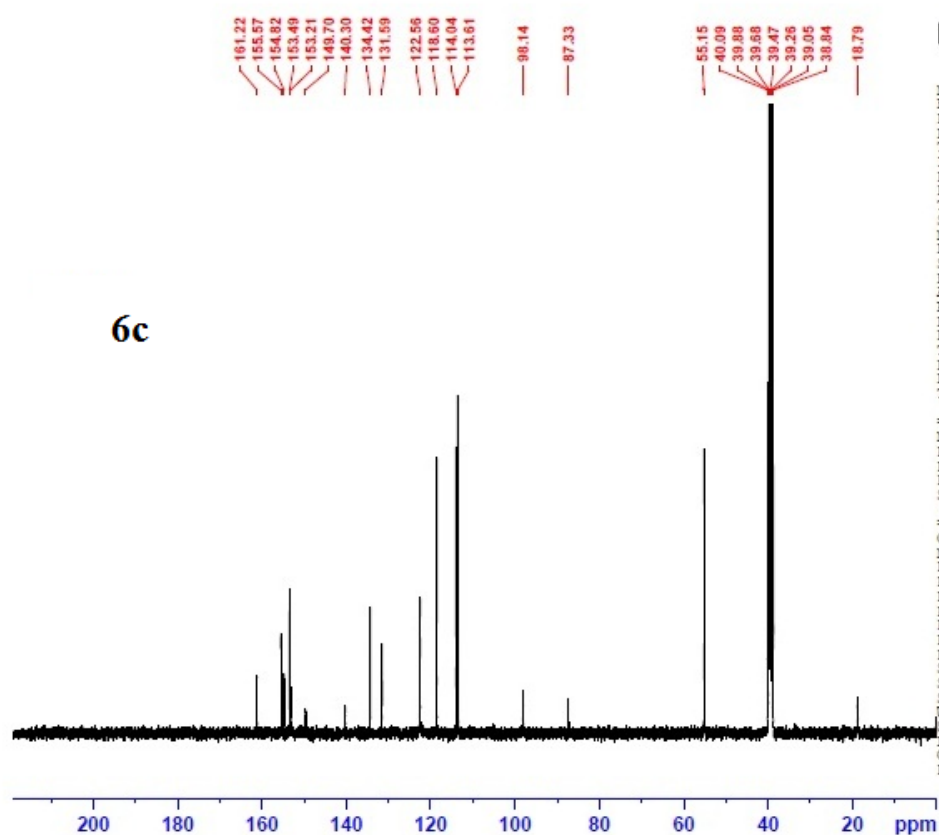EXPNO   1
PROCNO   1
Date_   20161206
Time   18.14
INSTRUM   spect
PROBHD   5 mm BBO BB-1H
PULPROG   zgpg30
TD   65536
SOLVENT   DMSO
NS   1024
DS   4
SWH   24038.461 Hz
FIDRES   0.366798 Hz
AQ   1.3631988 sec
RG   2050
DW   20.800 usec
DE   6.50 usec
TE   300.0 K
D1   2.00000000 sec
D11   0.03000000 sec
TD0   1

======== CHANNEL f1 ========
NUC1   13C
P1   10.00 usec
PL1   0.00 dB
PL1W   35.41759872 W
SFO1   100.6228298 MHz

======== CHANNEL f2 ========
CPDPRG2   waltz16
NUC2   1H
PCPD2   80.00 usec
PL2   0.00 dB
PL12   15.08 dB
PL13   18.08 dB
PL2W   8.31434441 W
PL12W   0.25812379 W
PL13W   0.12936834 W
SFO2   400.1316005 MHz
SI   32768
SF   100.6128193 MHz
WDW   EM
SSB   0
LB   1.00 Hz
GB   0
PC   1.40

6c

¹H NMR spectrum peaks: 11.916, 9.601, 8.859, 7.726, 7.714, 7.709, 7.703, 7.691, 7.585, 7.577, 7.571, 7.559, 7.554, 7.546, 7.164, 7.158, 7.141, 7.125, 7.119, 6.964, 6.956, 6.951, 6.939, 6.934, 6.925, 5.768, 3.751, 3.376, 2.507, 2.503, 2.349

Integrations: 1.00, 0.99, 1.02, 2.11, 2.12, 2.11, 2.14, 1.01, 3.18, 3.22

6c

¹³C NMR spectrum peaks: 161.22, 155.57, 154.82, 153.49, 153.21, 149.70, 140.30, 134.42, 131.59, 122.56, 118.60, 114.04, 113.61, 98.14, 87.33, 55.15, 40.09, 39.88, 39.47, 39.26, 39.05, 38.84, 18.79

6d

1H NMR spectrum

Peaks: 12.040; 9.578, 7.605, 7.597, 7.592, 7.579, 7.574, 7.566, 6.952, 6.947, 6.938, 6.933, 6.921, 6.916, 6.907, 5.744; 2.568, 2.527, 2.504, 2.342

NAME   PM-LMPM-30
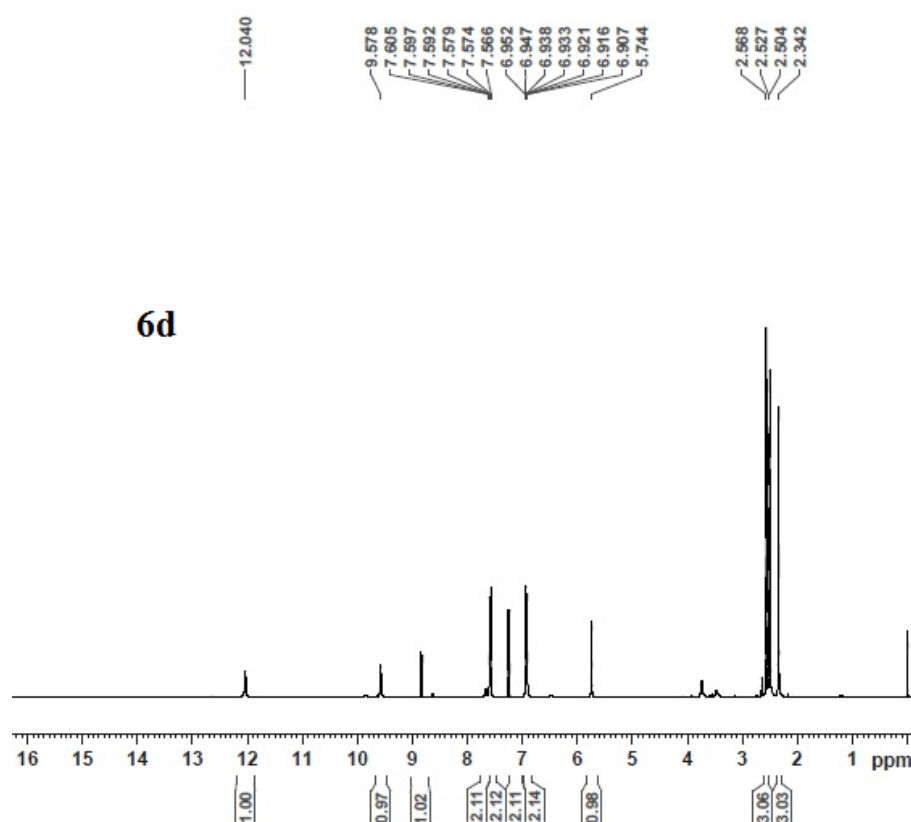EXPNO   1
PROCNO   1
Date_   20161206
Time   17.44
INSTRUM   spect
PROBHD   5 mm BBO BB-1H
PULPROG   zg30
TD   65536
SOLVENT   DMSO
NS   16
DS   2
SWH   8223.685 Hz
FIDRES   0.125483 Hz
AQ   3.9846387 sec
RG   203
DW   60.800 usec
DE   6.50 usec
TE   300.0 K
D1   1.00000000 sec
TD0   1

======== CHANNEL f1 ========
NUC1   1H
P1   14.10 usec
PL1   0.00 dB
PL1W   8.31434441 W
SFO1   400.1324710 MHz
SI   32768
SF   400.1300015 MHz
WDW   EM
SSB   0
LB   0.30 Hz
GB   0
PC   1.00

Integrations: 1.00; 0.97; 1.02; 2.11, 2.12, 2.11, 2.14; 0.98; 3.06, 3.03

6d

13C NMR spectrum

Peaks: 161.22, 155.57, 154.82, 153.49, 153.21, 149.70, 140.30, 134.42, 131.59, 122.56, 118.60, 114.04, 113.61, 98.14, 87.33, 55.15, 40.09, 39.88, 39.68, 39.47, 39.26, 39.05, 38.84, 18.79

NAME   PM-LMPM-30
EXPNO   1
PROCNO   1
Date_   20161206
Time   18.14
INSTRUM   spect
PROBHD   5 mm BBO BB-1H
PULPROG   zgpg30
TD   65536
SOLVENT   DMSO
NS   1024
DS   4
SWH   24038.461 Hz
FIDRES   0.366798 Hz
AQ   1.3631988 sec
RG   2050
DW   20.800 usec
DE   6.50 usec
TE   300.0 K
D1   2.00000000 sec
D11   0.03000000 sec
TD0   1

======== CHANNEL f1 ========
NUC1   13C
P1   10.00 usec
PL1   0.00 dB
PL1W   35.41759872 W
SFO1   100.6228298 MHz

======== CHANNEL f2 ========
CPDPRG2   waltz16
NUC2   1H
PCPD2   80.00 usec
PL2   0.00 dB
PL12   15.08 dB
PL13   18.08 dB
PL2W   8.31434441 W
PL12W 0.25812379 W
PL13W 0.12936834 W
SFO2   400.1316005 MHz
SI   32768
SF   100.6128193 MHz
WDW   EM
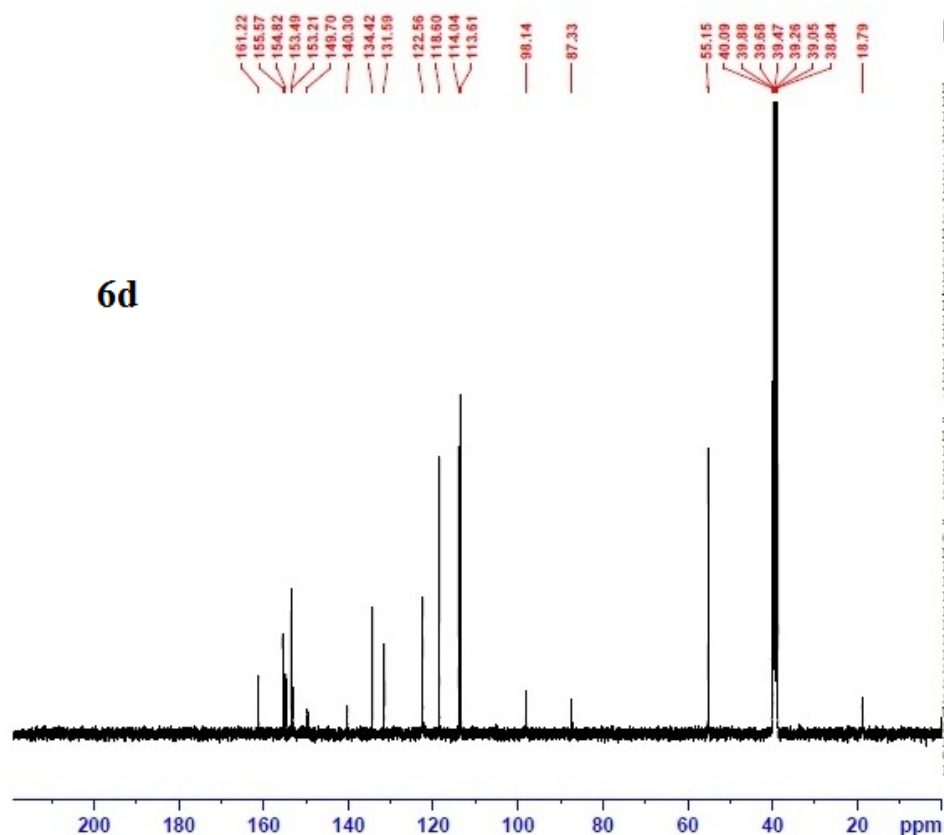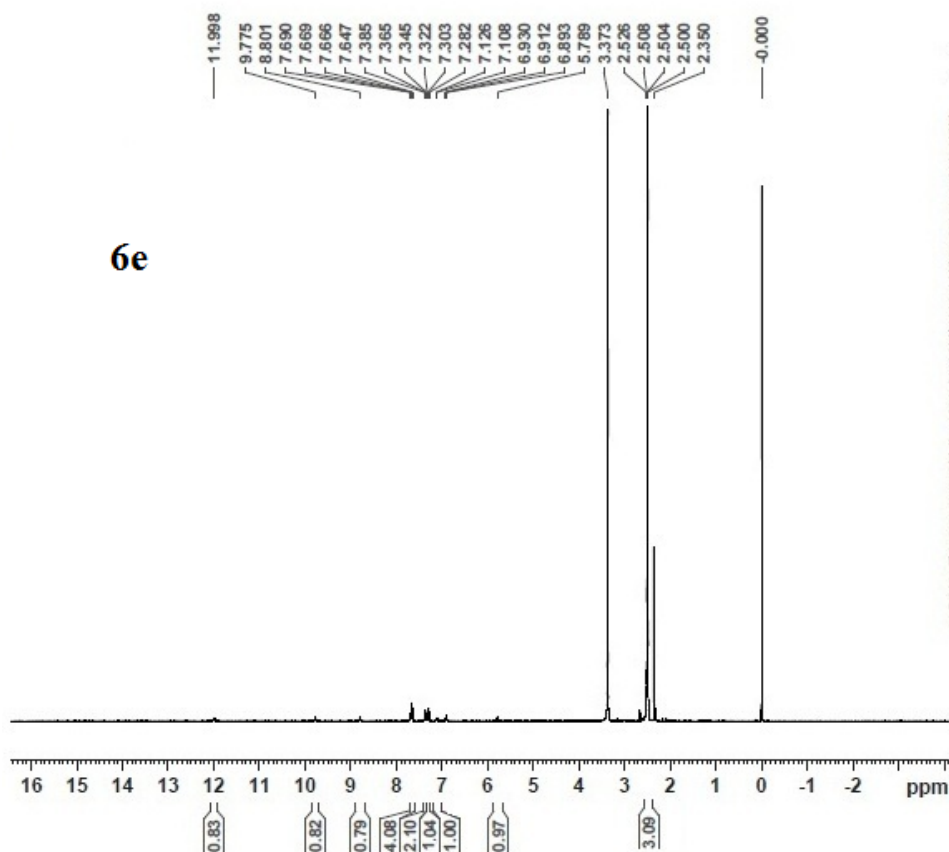SSB   0
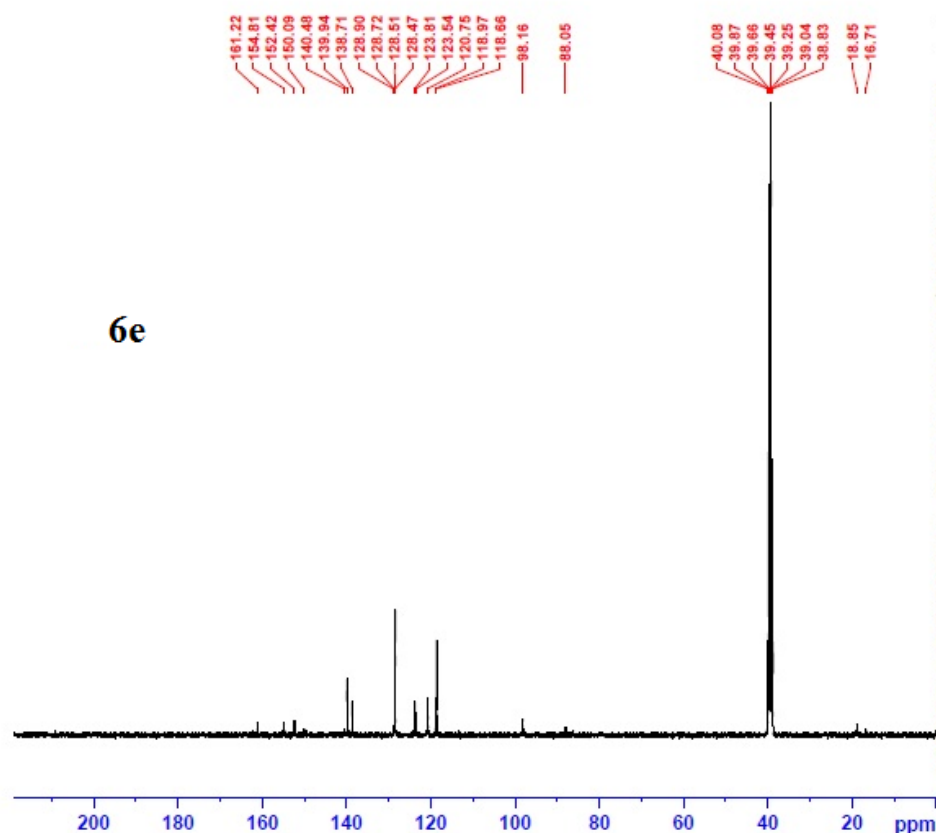LB   1.00 Hz
GB   0
PC   1.40

6e

11.998
9.775
8.801
7.690
7.669
7.666
7.647
7.385
7.365
7.345
7.322
7.303
7.282
7.126
7.108
6.930
6.912
6.893
5.789
3.373
2.526
2.508
2.504
2.500
2.350
-0.000

16 15 14 13 12 11 10 9 8 7 6 5 4 3 2 1 0 -1 -2 ppm

0.83
0.82
0.79
4.08
2.10
1.04
1.00
0.97
3.09

6e

161.22
154.81
152.42
150.09
140.48
139.94
138.71
128.90
128.72
128.51
128.47
123.54
123.81
120.75
118.97
118.66
98.16
88.05
40.08
39.87
39.66
39.45
39.25
39.04
38.83
18.85
16.71

200 180 160 140 120 100 80 60 40 20 ppm

6f

1H NMR peaks: 11.925, 9.714, 8.599, 7.661, 7.642, 7.615, 7.610, 7.598, 7.593, 7.381, 7.362, 7.342, 7.123, 7.105, 7.087, 6.907, 6.902, 6.889, 6.884, 5.761, 3.720, 2.506, 2.502, 2.345

Integrations: 1.00, 0.99, 1.04, 2.08, 2.13, 2.12, 1.07, 2.03, 1.03, 3.03, 3.18

6f

13C NMR peaks: 161.22, 154.81, 152.42, 150.09, 140.48, 139.94, 138.71, 128.90, 128.72, 128.51, 128.47, 123.81, 123.54, 120.75, 118.97, 118.66, 98.16, 88.05, 55.15, 40.08, 39.87, 39.66, 39.45, 39.25, 39.04, 38.83, 18.85

6g

¹H NMR peaks: 11.992, 9.919, 9.744, 9.249, 8.852, 8.285, 8.263, 8.235, 8.214, 7.830, 7.817, 7.808, 7.795, 7.665, 7.652, 7.643, 7.630, 7.276, 7.254, 7.247, 7.224, 7.202, 7.027, 7.000, 6.454, 5.800, 4.100, 4.082, 3.588, 3.508, 2.668, 2.503, 2.361, 2.324, 2.229, 2.233

NAME   PM-LMPM-33
EXPNO   1
PROCNO   1
Date_   20161206
Time   13.45
INSTRUM   spect
PROBHD   5 mm BBO BB-1H
PULPROG   zg30
TD   65536
SOLVENT   DMSO
NS   16
DS   2
SWH   8223.685 Hz
FIDRES   0.125483 Hz
AQ   3.9846387 sec
RG   256
DW   60.800 usec
DE   6.50 usec
TE   300.0 K
D1   1.00000000 sec
TD0   1

======== CHANNEL f1 ========
NUC1   1H
P1   14.10 usec
PL1   0.00 dB
PL1W   8.31434441 W
SFO1   400.1324710 MHz
SI   32768
SF   400.1300013 MHz
WDW   EM
SSB   0
LB   0.30 Hz
GB   0
PC   1.00

Integrals: 1.00, 1.00, 1.04, 2.02, 2.08, 2.04, 2.08, 1.02, 3.09

6g

¹³C NMR peaks: 161.38, 157.71, 155.36, 154.74, 152.61, 150.01, 140.67, 140.37, 137.43, 132.76, 130.15, 123.02, 119.93, 118.86, 118.75, 118.68, 115.27, 115.05, 98.27, 87.73, 40.09, 39.88, 39.67, 39.46, 39.25, 39.04, 38.84, 18.85

NAME   PM-LMPM-33
EXPNO   2
PROCNO   1
Date_   20160519
Time   16.14
INSTRUM   spect
PROBHD   5 mm BBO BB-1H
PULPROG   zgpg30
TD   65536
SOLVENT   DMSO
NS   922
DS   4
SWH   24038.461 Hz
FIDRES   0.366798 Hz
AQ   1.3631988 sec
RG   2050
DW   20.800 usec
DE   6.50 usec
TE   300.0 K
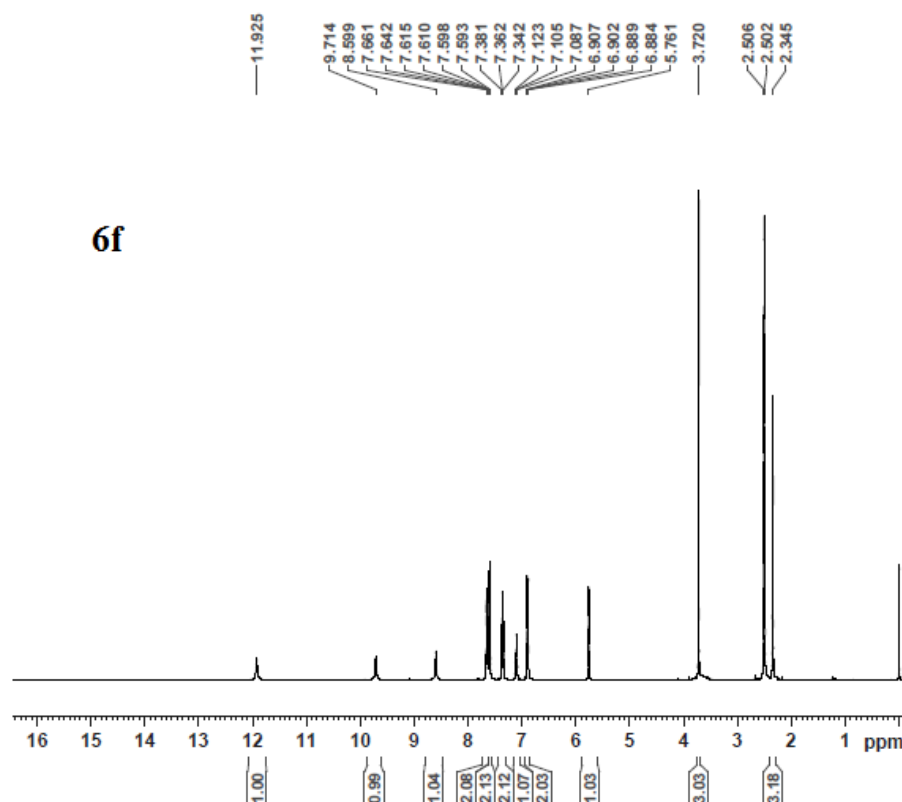D1   2.00000000 sec
D11   0.03000000 sec
TD0   1

======== CHANNEL f1 ========
NUC1   13C
P1   10.00 usec
PL1   0.00 dB
PL1W   35.41759872 W
SFO1   100.6228298 MHz

======== CHANNEL f2 ========
CPDPRG2   waltz16
NUC2   1H
PCPD2   80.00 usec
PL2   0.00 dB
PL12   15.08 dB
PL13   18.08 dB
PL2W   8.31434441 W
PL12W   0.25812379 W
PL13W   0.12936834 W
SFO2   400.1316005 MHz
SI   32768
SF   100.6128193 MHz
WDW   EM
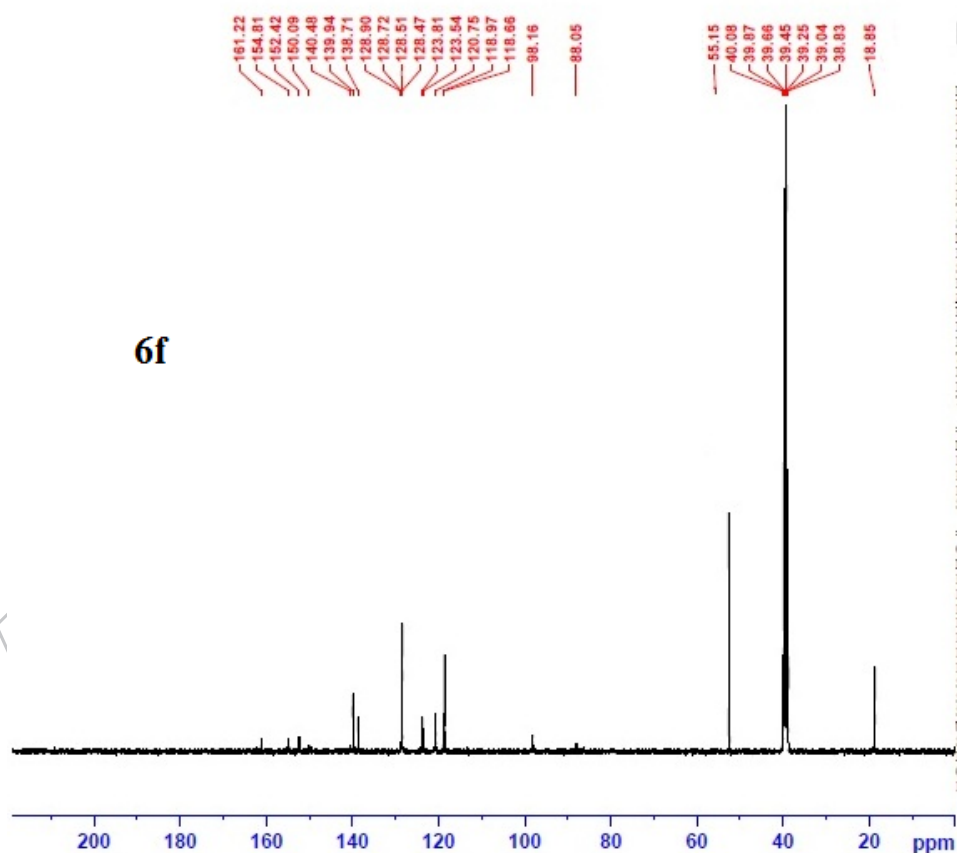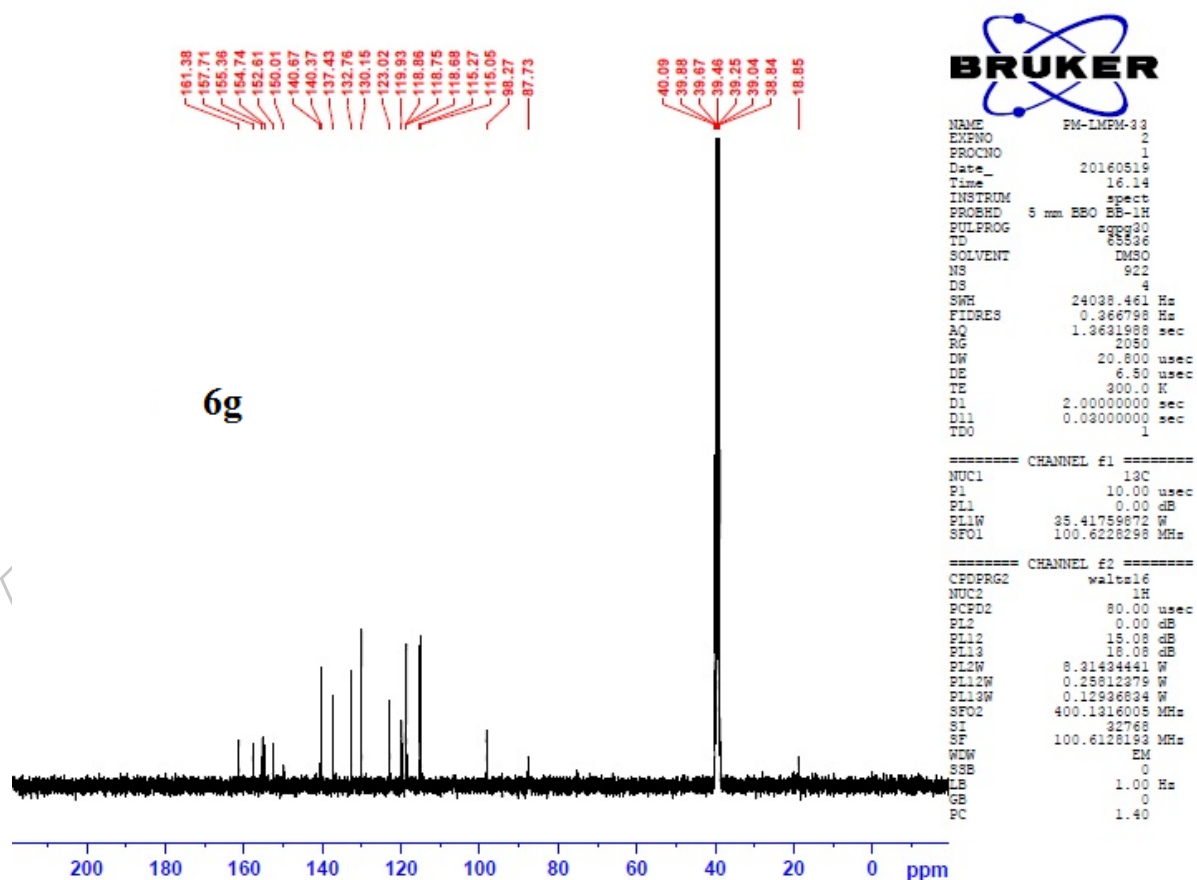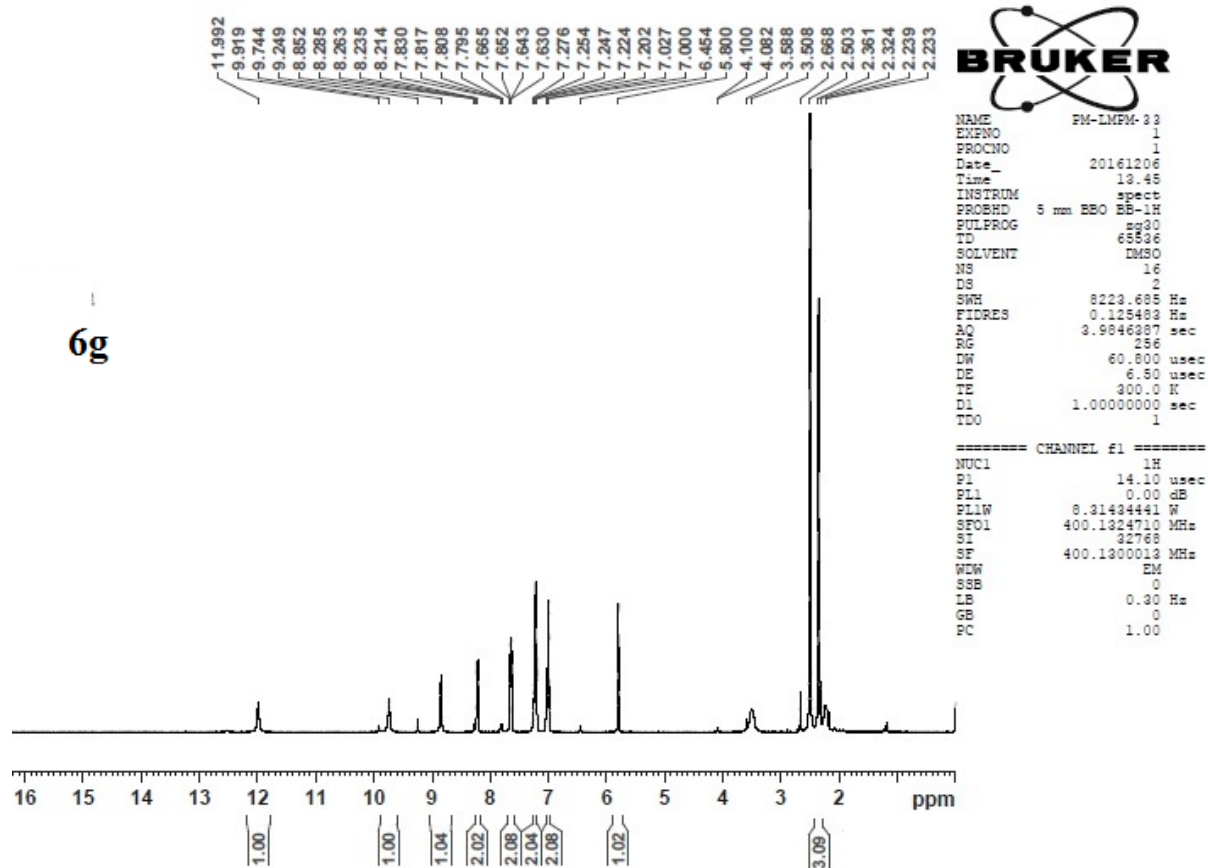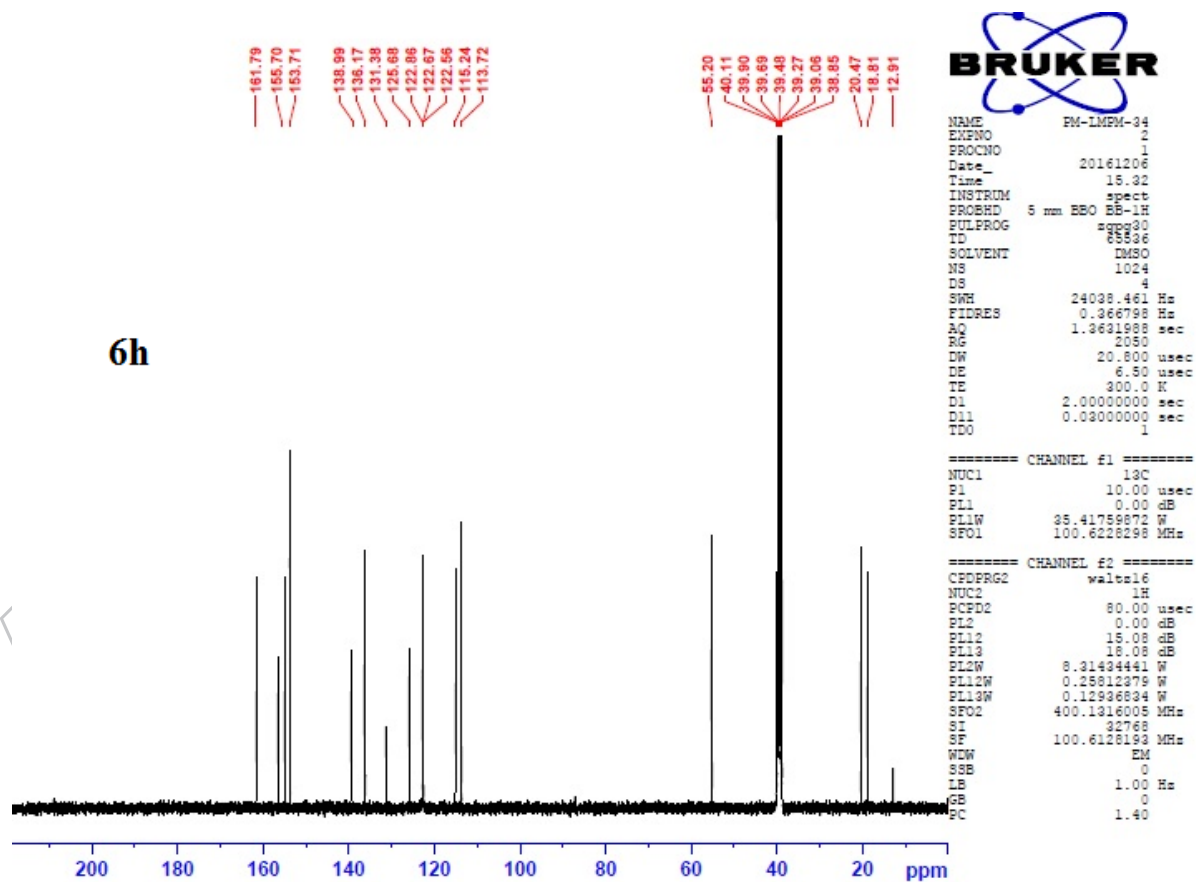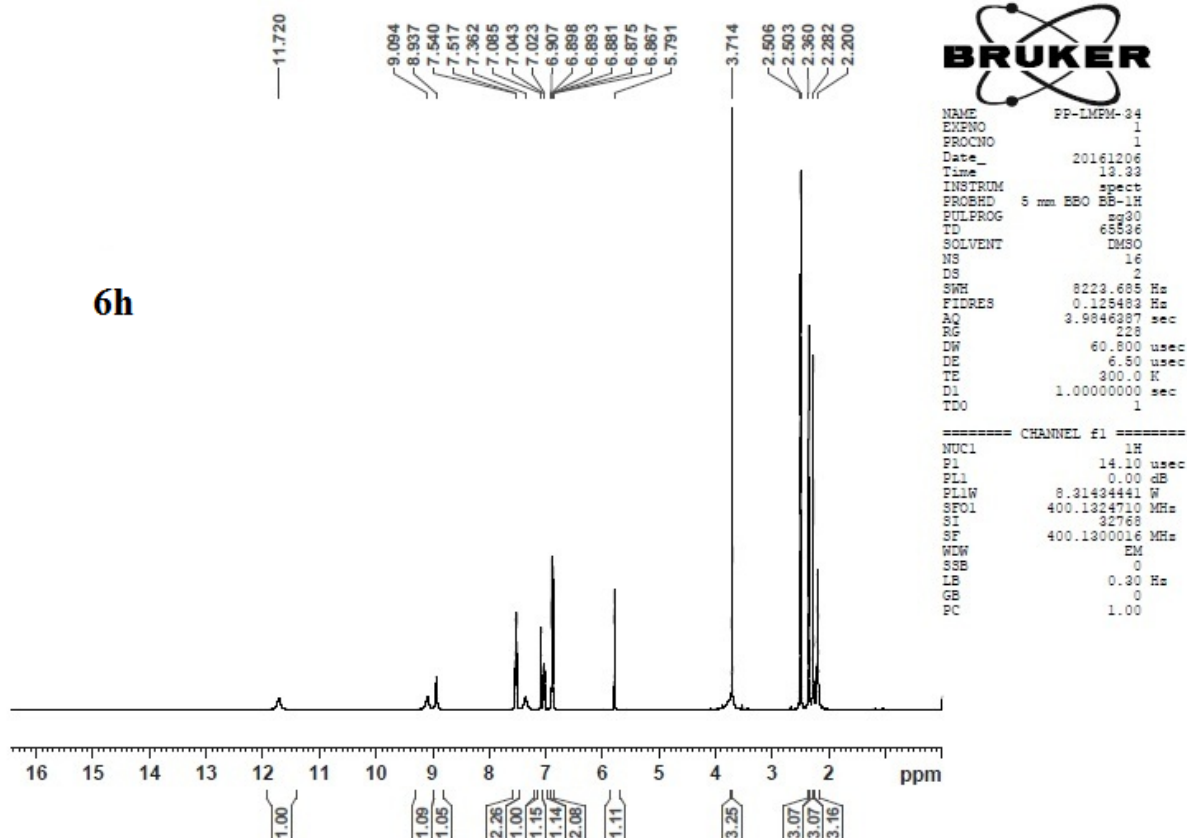SSB   0
LB   1.00 Hz
GB   0
PC   1.40

6h

11.720
9.094
8.937
7.540
7.517
7.362
7.085
7.043
7.023
6.907
6.898
6.893
6.881
6.875
6.867
5.791
3.714
2.506
2.503
2.360
2.282
2.200

NAME   PP-LMPM-34
EXPNO   1
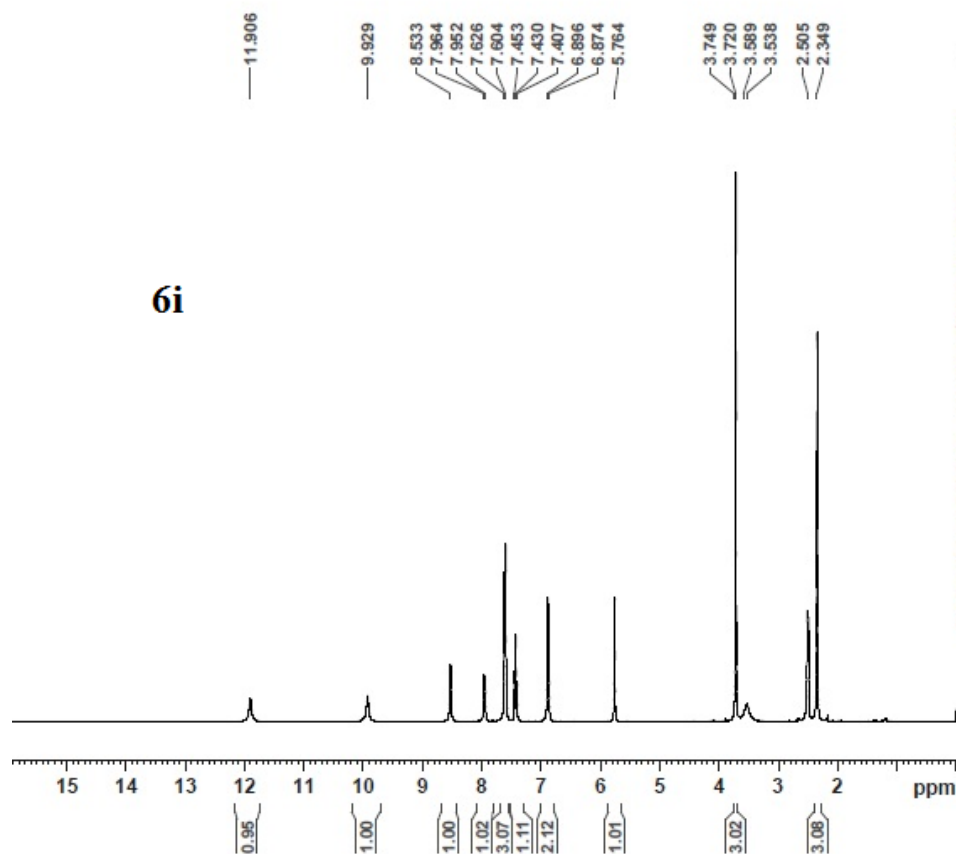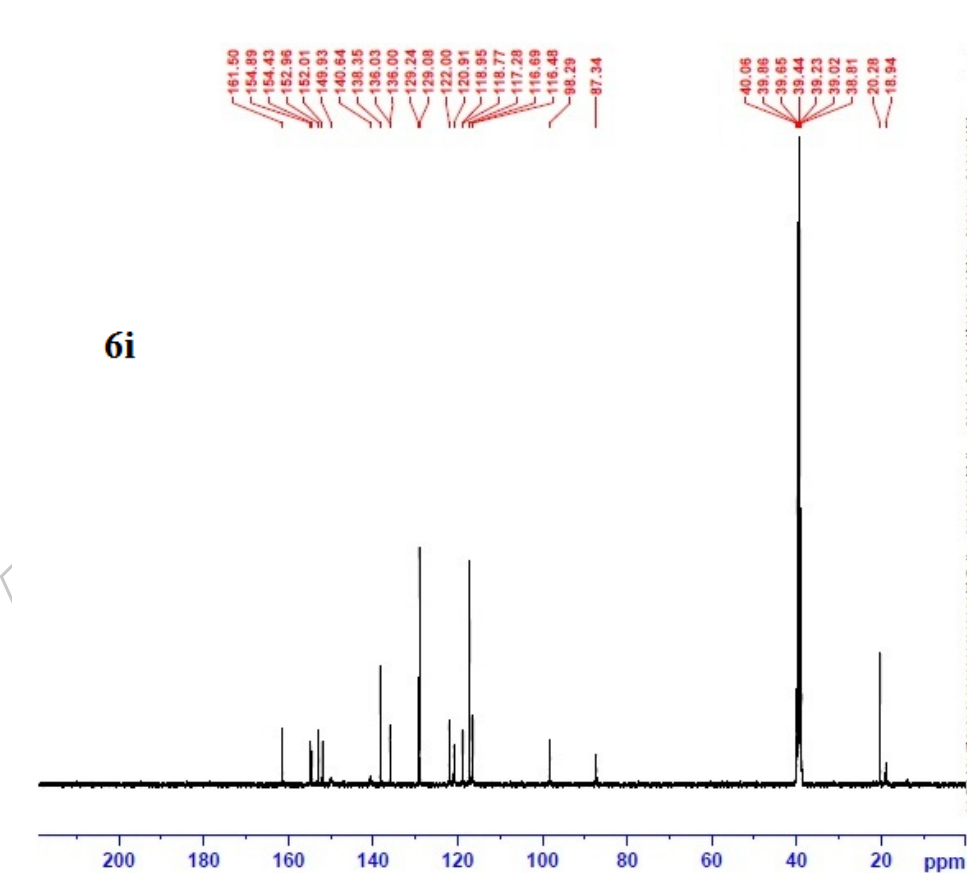PROCNO   1
Date_   20161206
Time   13.33
INSTRUM   spect
PROBHD   5 mm BBO BB-1H
PULPROG   zg30
TD   65536
SOLVENT   DMSO
NS   16
DS   2
SWH   8223.685 Hz
FIDRES   0.125483 Hz
AQ   3.9846387 sec
RG   228
DW   60.800 usec
DE   6.50 usec
TE   300.0 K
D1   1.00000000 sec
TD0   1

======== CHANNEL f1 ========
NUC1   1H
P1   14.10 usec
PL1   0.00 dB
PL1W   8.31434441 W
SFO1   400.1324710 MHz
SI   32768
SF   400.1300016 MHz
WDW   EM
SSB   0
LB   0.30 Hz
GB   0
PC   1.00

1.00
1.09
1.05
2.26
1.00
1.15
1.14
2.08
1.11
3.25
3.07
3.07
3.16

6h

161.79
155.70
153.71
138.99
136.17
131.38
125.68
122.86
122.67
122.56
115.24
113.72
55.20
40.11
39.90
39.69
39.48
39.27
39.06
38.85
20.47
18.81
12.91

NAME   PM-LMPM-34
EXPNO   2
PROCNO   1
Date_   20161206
Time   15.32
INSTRUM   spect
PROBHD   5 mm BBO BB-1H
PULPROG   zgpg30
TD   65536
SOLVENT   DMSO
NS   1024
DS   4
SWH   24038.461 Hz
FIDRES   0.366798 Hz
AQ   1.3631988 sec
RG   2050
DW   20.800 usec
DE   6.50 usec
TE   300.0 K
D1   2.00000000 sec
D11   0.03000000 sec
TD0   1

======== CHANNEL f1 ========
NUC1   13C
P1   10.00 usec
PL1   0.00 dB
PL1W   35.41759872 W
SFO1   100.6228298 MHz

======== CHANNEL f2 ========
CPDPRG2   waltz16
NUC2   1H
PCPD2   80.00 usec
PL2   0.00 dB
PL12   15.08 dB
PL13   18.08 dB
PL2W   8.31434441 W
PL12W   0.25812379 W
PL13W   0.12936834 W
SFO2   400.1316005 MHz
SI   32768
SF   100.6128193 MHz
WDW   EM
SSB   0
LB   1.00 Hz
GB   0
PC   1.40

6i

6i